Available online at www.sciencedirect.com
SCIENCE DIRECT®
Journal of African Earth Sciences 40 (2004) 115–136
Journal of African Earth Sciences
www.elsevier.com/locate/jafrearsci

The Pan-African high-K calc-alkaline peraluminous Elat granite from southern Israel: geology, geochemistry and petrogenesis

M. Eyal [a], B.A. Litvinovsky [a,b,*], Y. Katzir [a], A.N. Zanvilevich [a]

[a] *Department of Geological and Environmental Sciences, Ben-Gurion University of the Negev, P.O. Box 653, Beer-Sheva 84105, Israel*
[b] *Geological Institute, RAS, Ulan-Ude, Russia*

Received 28 July 2003; received in revised form 29 September 2004; accepted 19 November 2004

Abstract

Calc-alkaline leucocratic granites that were emplaced at the late post-collision stage of the Pan-African orogeny are abundant in the northern half of the Arabian-Nubian Shield. Commonly, they are referred to as the Younger Granite II suite. In southern Israel such rocks are known as Elat granite. Studies of these rocks enable to recognize two types of granites: coarse-grained, massive Elat granite (EG), and fine- to medium-grained Shahmon gneissic granite (SGG). Both granite types are high-K and peraluminous (*ASI* ranges from 1.03 to 1.16). They are similar in modal composition, mineral and whole-rock chemistry. Within the EG, a noticeable distinction in whole-rock chemistry and mineral composition is observed between rocks making up different plutons. In particular, the granite of Wadi Shelomo, as compared to the Rehavam pluton, is enriched in SiO_2, FeO*, K_2O, Ba, Zr, Th, LREE and impoverished in MgO, Na_2O, Sr, and HREE. The Eu/Eu* values in the granite are low, up to 0.44. Mass-balance calculations suggest that chemical and mineralogical variations were caused by fractionation of ~16 wt.% plagioclase from the parental Rehavam granite magma at temperature of 760–800 °C (muscovite-biotite geothermometer). The Rb-Sr isochrons yielded a date of 623 ± 24 Ma for the EG, although high value of age-error does not allow to constrain time of emplacement properly. The Rb-Sr date for SGG is 640 ± 9 Ma; however, it is likely that this date points to the time of metamorphism. A survey of the literature shows that peraluminous, high-K granites, similar to the EG, are abundant among the Younger Granite II plutons in the Sinai Peninsula and Eastern Desert, Egypt. They were emplaced at the end of the batholithic (late post-collision) stage. The most appropriate model for the generation of the peraluminous granitic magma is partial melting of metapelite and metagreywacke.

Keywords: Calc-alkaline leucocratic granite; Peraluminous; High-K; Arabian-Nubian Shield; Southern Israel

1. Introduction

Basement outcrops in southern Israel and southern Jordan comprise the northernmost part of the Arabian-Nubian Shield (Fig. 1, Inset). The Shield evolved through four main stages (Brown, 1980; Fleck et al., 1980; Gass, 1982; Roobol et al., 1983; Bentor, 1985; Stern and Hedge, 1985; Stern et al., 1988; Kröner et al., 1990; Genna et al., 2002). During the *first and second stages* (~950–850 Ma and 850–650 Ma respectively), oceanic crust and island arcs were formed. Tholeiitic basalt, gabbro and trondhjemite followed by andesitic to dacitic rocks and their plutonic equivalents, as well as sedimentary derivates, were produced in those stages. At the end of the second stage, oceanic and island arc terrains were amalgamated and accreted to form the Arabian-Nubian Shield. The post-collision *batholithic stage* 3 (~650–580 Ma) marks stabilization of the Shield and is characterized by widespread calc-alkaline magmatism, mainly of intermediate to felsic composition. At the boundary between stages 3 and 4 a fundamental

* Corresponding author. Tel.: +972 8 6477522.
E-mail addresses: moey@bgumail.bgu.ac.il (M. Eyal), borisl@bgumail.bgu.ac.il (B.A. Litvinovsky).

0899-5362/$ - see front matter © 2004 Elsevier Ltd. All rights reserved.
doi:10.1016/j.jafrearsci.2004.11.005

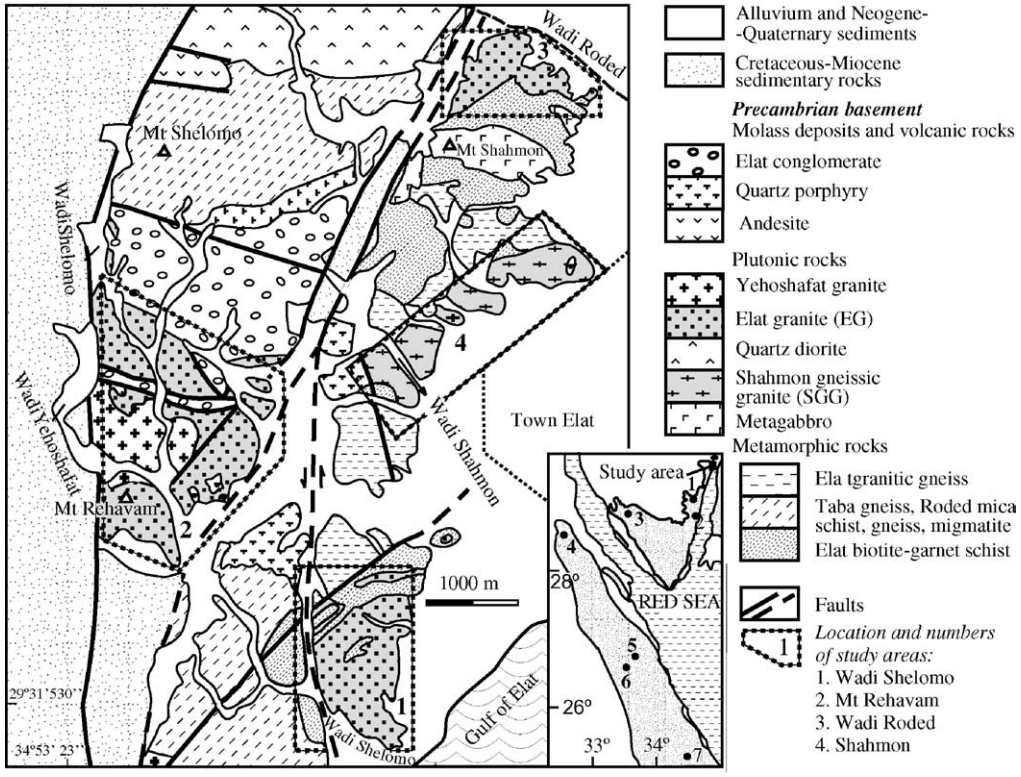

Fig. 1. The geological map of the Elat block, southern Israel (after Druckman et al., 1993; Garfunkel et al., 2000, with authors' modifications). In the Inset, stippled areas are exposures of the Pan-African basement. The localities of late to post-collisional calc-alkaline Younger Granite II that are considered in the "Discussion" are shown: 1—Nuweiba area, eastern Sinai (Ahmed et al., 1993); 2—Wadi Risasa area, southeastern Sinai (El-Sheshtawi et al., 1993); 3—southwestern Sinai (El-Mettwaly et al., 1992); 4—Wadi Hawashia, north of Eastern Desert (Mohamed et al., 1994); 5—Gabal El-Urf area, Eastern Desert (Moghazi, 1999); 6—Mt El-Sibai, Eastern Desert (Abdel-Rahman and El-Kibbi, 2001); 7—Wadi El-Imra district, Central Eastern Desert (Furnes et al., 1996).

transition in tectonic style, from compressional to extensional, occurred about 600 Ma (Stern and Hedge, 1985; Garfunkel, 2000). The *post-orogenic stage* 4 (~600–530 Ma) involves igneous activity of mainly alkaline to peralkaline granites, andesites, rhyolites and several episodes of dike swarms representing late post-orogenic intracratonic within-plate magmatism.

The calc-alkaline granitoids formed during the batholithic stage are the most abundant plutonic rocks in the northern part of the Arabian-Nubian Shield. Two suites of calc-alkaline granitoids are usually recognized: older diorite-tonalite-granodiorite (Granite I) and younger granite suites. The latter is referred to in the Sinai Peninsula and Eastern Desert (Egypt) as Younger Granite II, calc-alkaline younger biotite granite, younger post-tectonic granite or late-tectonic monzogranite (El-Mettwaly et al., 1992; El-Sheshtawi et al., 1993; Ahmed et al., 1993; Mohamed et al., 1994; Furnes et al., 1996; Moghazi, 1999, 2002; Abdel-Rahman and El-Kibbi, 2001). In southern Israel similar rocks are known as Elat granite (Bentor and Vroman, 1955; Bentor, 1961).

In this paper we present data on the petrography, mineral and whole-rock chemistry, Rb–Sr and oxygen isotopic data from the Elat granite. Also the Shahmon gneissic granite (SGG) that was previously considered as EG is described. Both EG and SGG are high-K and peraluminous. It is shown that high-K, peraluminous granites similar to the Elat type are abundant among the Pan-African calc-alkaline granitic rocks in the Sinai Peninsula and Eastern Desert, Egypt.

2. Geological setting

The EG is abundant in southern Israel (Fig. 1, see also Garfunkel et al., 2000). Exposures occur in small areas ranging from 1.5 to 3 km^2; they are overlain unconformably by Late Neoproterozoic volcanic rocks and conglomerate and by Neogene to Recent sediment rocks. The EG is intruded by the alkaline Yehoshafat granite. Country rocks are biotite-garnet Elat schists and granitic gneisses formed ~800 and 740 Ma respectively (Eyal et al., 1991). Four areas with the largest granite exposures have been studied in detail: (1) Wadi Shelomo, (2) Mt Rehavam, (3) Wadi Roded, and (4) the area south of Mt Shahmon (Fig. 1).

The Wadi Shelomo pluton is made up of homogeneous massive biotite, in places garnet-bearing, monzo-

granite that intrudes the Elat schist. Numerous pegmatite veins and vein networks making up about 5% of the total volume are characteristic of the pluton. Veins are mostly gently dipping (10°–15° in various directions). Their thickness ranges from a few cm to 1 m. Pegmatite veins are also common in the country rocks, mostly near the contact with the granite pluton. Abundance of pegmatites, as well as the presence of fairly large, about 100 m across, schist xenoliths in the upper level of the granite exposure, suggest a comparatively shallow depth of erosion of the pluton.

The granite exposures in the Mt Rehavam and Wadi Roded areas are interpreted as two parts of a single pluton. The pluton was cut by a Neogene fault and its eastern part (Wadi Roded area) underwent about 6 km displacement to the north along the shear zone (Eyal and Peltz, 1994). These two parts taken together are named the Rehavam pluton, which consists of coarse-grained two-mica monzogranite. In the western part (Mt Rehavam area) the monzogranite is homogeneous in texture and mineral composition throughout the hypsographic relief of 300 m. Pegmatite veins are extremely rare and xenoliths of country rocks are absent suggesting that the granitic pluton in this area is eroded to a deeper level than in the Wadi Shelomo pluton. In the Wadi Roded area, the contact zone of the pluton adjacent to the enclosing biotite-garnet schist is significantly enriched in muscovite-garnet-bearing pegmatite veins. Immediately near the contact the granite texture becomes pegmatitic.

The main feature of the contact zones both in the Wadi Shelomo and Wadi Roded areas is the abundance of conformable, mostly gently SE-dipping dike- and sill-like monzogranite apophyses in the schist. The thickness of apophyses ranges from less than 1 cm to several tens of meters. Although penetration of schist by the magmatic material was very extensive (granite veins range up to 60% of total volume), evidence of assimilation or exchange reactions between magmatic and metamorphic rocks is very scarce. The mineral assemblages near the contact with magmatic rocks are actually the same as far away from the contact. No evidence of partial melting in schist (e.g., lensoid patches of newly formed granite, evidence of biotite breakdown) is found.

In the area to the south of Mt Shahmon, the Elat granites are recognized in a number of geological maps, including the latest 1:100 000 Geological map of the northern Gulf of Elat area (Garfunkel et al., 2000). However, our field and analytical studies show that, contrary to the common EG, gneissic texture is characteristic of granite in this area. We call them Shahmon gneissic granite (SGG). The SGG is a two-mica rock exposed in an area ~2.5 km in length and <1 km wide. Most outcrops consist of weakly gneissic, fine- to medium-grained granite; granite with clear gneissic texture is present only in the SW part of the exposure. The gneissosity is mostly steeply dipping and vertical, with dominant EW strike. The contact between the two varieties is fairly sharp, but without any evidence of crosscutting relationships. Veins of muscovite-garnet-bearing pegmatites are rare. Country rocks are Elat granitic gneiss, biotite-garnet and staurolite Elat schists. The granite exposures are overlain by the Quaternary cover.

3. Analytical methods

Microprobe mineral analyses were carried out using a four-channel MAR-3 electron probe microanalyser at the Geological Institute, Siberian Branch of the Russian Academy of Sciences, Ulan-Ude. Analyses were obtained with a beam of 2–3 μm in diameter. Operating conditions were 20 kV, 40 μA beam current, and a counting time of 10 s. The detection limits are 0.05–0.09 wt.% for Na_2O, MgO, Al_2O_3, and SiO_2; 0.01–0.05 wt.% for Cl, K_2O, CaO, TiO_2, MnO and FeO; 0.06–0.15 wt.% for BaO; 0.3–0.4 wt.% for SrO and F.

Whole-rock chemical analyses were made using a combination of wet chemical methods, AAS and titration (major elements), and X-ray fluorescence (Rb, Sr, Ba, Y, Zr and Nb) at the Geological Institute, Ulan-Ude. Rare earth and some selected trace elements (Hf, Ta, Th, U, Ga, V, Cu, Pb, Zn, Sc and Cs) were analyzed by ICP-MS at the Institute of Mineralogy and Geochemistry of Rare Elements, Moscow. Analyses are considered accurate to within 2–5% for major elements, and better than 10–15% for trace elements. The accuracy for all the REE (except Lu) is 1–5%; for Lu, it is 9–10%. Normalizing trace element concentrations for chondrite are from Sun and McDonough (1989). Major and trace elements were determined for 61 samples; REE were measured in 13 samples.

Rb–Sr isotope ratios were measured at the Geological Institute, Ulan-Ude on MI-1202 T mass spectrometer, in a single-ray mode. The isotopic composition and concentration of Sr were determined by the method of double isotopic dilution, and Rb content, by isotopic dilution. The measurement of Sr isotopic compositions was controlled using the standard VNIIM (attested value $^{87}Sr/^{86}Sr = 0.70801$), which yielded $^{87}Sr/^{86}Sr = 0.70796 \pm 0.00009$ in the course of the measurements. The uncertainties of isotopic ratios were determined taking into account parallel measurements of $^{87}Sr/^{86}Sr$ and $^{87}Rb/^{86}Sr$ as no higher than 0.05 and 2%, respectively. Ages were calculated by the York method using the ISOPLOT program (Ludwig, 2003).

Oxygen isotope analyses were performed using the laser fluorination technique at the University of Wisconsin, Madison, USA. Oxygen was liberated by reaction with BrF_5, purified cryogenically and with an in-line Hg diffusion pump, converted to CO_2 on a hot graphite

rod, and analyzed on a Finnigan MAT 251 mass spectrometer (Valley et al., 1995). Quartz separates were analyzed using the rapid heating, defocused beam technique (Spicuzza et al., 1998). Average reproducibility for quartz is 0.09‰ and for zircon and garnet 0.02‰. On each analysis day at least four aliquots of UW Gore Mountain Garnet standard (UWG-2) were analyzed. The overall average for UWG-2 during the period of the study was 5.61 ± 0.09‰. $\delta^{18}O$ values of samples were adjusted by an average of 0.19‰, the difference between each day's UWG-2 value and 5.8‰, the accepted value of UWG-2.

4. Petrography

4.1. The Elat granites

The EG is leucocratic pinkish to light gray, medium- to coarse-grained and in places porphyritic. According to the modal composition (Table 1; Fig. 2), they are monzogranites (Le Maitre, 1989). Accessory minerals are monazite, zircon and magnetite, with rare apatite and titanite.

Monzogranite from the Rehavam pluton is a coarse-grained (5–8 mm) two-mica rock of hypidiomorphic texture, with a dominance of plagioclase over alkali feldspar (Table 1; Fig. 2). It contains 2.5–5.0 vol.% of biotite and 2.5–3.0 vol.% muscovite in 1–1.5 mm long euhedral to subhedral flakes. Prismatic crystals of plagioclase are commonly compositionally zoned (An_{13} in the cores and An_6 in thin rims). Quartz and alkali feldspar occur as anhedral and interstitial grains. Alkali feldspar has irregular vein-patch perthite texture with about 20–30 vol.% of *Ab* phase. Secondary muscovite is also present, it forms small flakes dispersed within the feldspar grains, and rarely within the biotite flakes.

Monzogranite from the Wadi Shelomo pluton, unlike the Rehavam pluton, is richer in quartz and alkali feldspar (Table 1; Fig. 2). The distinctive textural feature of this monzogranite is partial resorption of plagioclase by alkali feldspar, commonly with myrmekitic intergrowths. The plagioclase grains ($An_{12–15}$) are mostly unzoned, in places weakly zoned. Alkali feldspar is similar to that in the Rehavam monzogranite. Biotite occurs in euhedral flakes and elongated aggregates. Muscovite is practically absent. Rare spessartine–almandine garnet crystals are found in close proximity to the garnet-rich pegmatite veins.

4.2. The Shahmon gneissic granites

The main feature of rocks of this type is the gneissic texture. Two rock varieties, weakly and strongly gneissic, are distinguished; the former is dominant. Both varieties are two-mica rocks with typical hypidiomorphic texture. By modal composition they are monzogranite with approximately equal amounts (3.5–4.5 vol.%) of biotite and muscovite (Table 1; Fig. 2). Accessory minerals, zircon, titanite, apatite and magnetite, constitute about 0.5% of the rock volume.

Weakly gneissic monzogranite is fine- to medium-grained (from 0.5 to 1.5 mm), of gray or bluish-gray colour. The rock is mostly even-grained, but rare plagioclase and alkali-feldspar phenocrysts about 3 by 4 mm are observed. Gneissic texture is commonly distinguished in hand specimens rather than in thin sections. Weak orientation of mica flakes and aggregates of quartz grains can be seen in a few thin sections. Prismatic crystals of plagioclase are commonly zoned (An_{14} in the core and $An_{6–9}$ in the rim); alkali feldspar and quartz are present as anhedral, in places interstitial, grains.

Table 1
Modal composition of representative Elat granite and Shahmon gneissic granite (vol.%)

Pluton	Rehavam (Mt Rehavam area)				Rehavam (Wadi Roded area)			Wadi Shelomo					
Sample no.	A38	A39	A101	A102	A41	A44	A48	A4	A6	A9	A24	A29	A33
Elat granite													
Quartz	26.5	31.5	30	29.5	31.5	31.5	31.5	36	34	39	34.5	36	37.5
Plagioclase	37	36	36.5	36	36	37	34	28	27	21.5	26.5	22	27
Alkali feldspar	30.5	26	26	25	26	25	28	30.5	33.5	33	34.5	35	30.5
Biotite	2.5	3.5	4	5	2.5	3	2.5	4.5	4.8	4	3.5	5.5	4.8
Muscovite	2.5	2.5	2	3	3.5	2.5	3	-	trace	-	-	trace	-

	Shahmon (weakly gneissic granite)					Shahmon (gneissic granite)			
	A50	A57	A-58	A89-1	A-99	A89	A112a	A112a-1	A114
Shahmon gneissic granite									
Quartz	32	32	32.5	33.5	30.5	29.5	32	30	30.5
Plagioclase	39	35	37	34.5	38	39	36	38	34
Alkali feldspar	22	25	23	24	24	24	24	23.5	26
Biotite	4	4	3	4	3.5	3.5	3.5	4.5	4.5
Muscovite	2.5	3	3.5	3.5	3.5	3.5	3.5	3.5	4.5

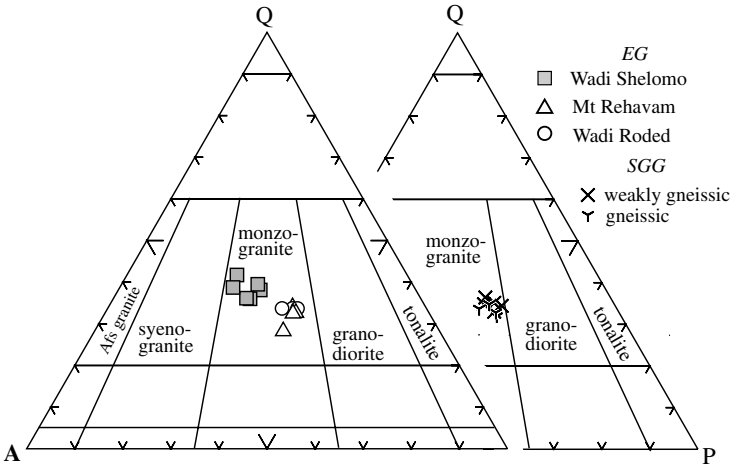

Fig. 2. Modal compositions of the EG and SGG plotted in QAP classification diagram.

Gneissic monzogranite is a pinkish-gray, dominantly medium-grained rock. In spite of gneissosity, patches with magmatic texture are abundant. The rock is porphyritic with plagioclase and alkali feldspar phenocrysts of 8–10 mm in length (5–7 vol.%). Plagioclase forms prismatic zoned (An_{12-14} in the core and An_{6-8} in the rim) and unzoned (An_{9-13}) crystals. Quartz and alkali feldspar grains are anhedral. Biotite is almost

Table 2
Microprobe analyses of biotite from the EG, SGG and from the enclosing biotite-garnet schists (wt.%)

Sample no.	A39	A38	A102	A41	A48	A4	A9	A29	A99	A50	A34	A107-1
Pluton/rock	Rehavam, EG					Wadi Shelomo, EG			Shahmon, SGG		Schist	
Area	Mt Rehavam			Wadi Roded							Wadi Shelomo	Wadi Roded
n	1	1	1	1	1	1	1	1	2	2	2	2
SiO_2	35.99	36.56	35.01	37.03	35.36	33.67	34.15	34.82	34.96	36.07	34.79	35.67
TiO_2	2.62	2.56	2.47	2.31	2.38	2.73	2.90	3.05	2.72	3.01	2.33	1.97
Al_2O_3	16.45	16.45	17.03	17.27	17.77	18.45	17.57	18.62	18.08	17.51	19.01	19.37
FeO*	20.19	19.39	23.42	19.99	21.18	27.65	28.43	26.52	24.40	22.49	21.16	19.16
MnO	0.93	0.84	0.74	1.08	0.86	0.50	0.50	0.55	0.73	0.58	0.13	0.11
MgO	9.58	9.76	7.11	7.34	7.79	3.94	3.77	4.00	5.53	6.63	8.56	9.23
CaO	0.12	0.09	-	0.23	0.06	0.06	0.11	0.04	0.02	0.06	0.05	0.33
Na_2O	0.11	0.07	-	0.09	0.09	0.13	0.13	0.22	0.07	0.07	0.26	0.09
K_2O	9.56	9.36	9.68	9.74	9.38	9.55	9.24	9.78	10.08	9.34	9.08	9.35
BaO	-	0.37	0.31	-	-	-	0.07	-	0.05	0.28	0.08	0.19
F	1.24	1.82	0.78	1.88	1.20	0.65	0.49	0.56	1.63	0.91	0.21	-
	96.79	97.26	96.56	96.93	96.07	97.33	97.35	98.17	98.28	96.95	95.66	
O=F	0.52	0.76	0.33	0.79	0.50	0.27	0.20	0.24	0.68	0.38	0.09	
Total	96.06	96.20	96.11	95.84	95.37	96.96	97.07	97.84	97.33	96.43	95.53	95.46
						Atoms to 11 oxygens						
Si	2.763	2.797	2.732	2.845	2.741	2.650	2.689	2.693	2.713	2.775	2.669	2.707
Al^{iv}	1.237	1.203	1.268	1.155	1.259	1.350	1.311	1.307	1.288	1.226	1.331	1.293
Al^{vi}	0.252	0.280	0.298	0.409	0.365	0.361	0.320	0.390	0.366	0.362	0.388	0.439
Ti^{vi}	0.151	0.147	0.145	0.133	0.139	0.162	0.172	0.177	0.159	0.175	0.135	0.113
Fe	1.296	1.240	1.529	1.284	1.373	1.820	1.872	1.715	1.583	1.448	1.358	1.217
Mn	0.060	0.054	0.049	0.070	0.056	0.033	0.033	0.036	0.048	0.038	0.009	0.008
Mg	1.096	1.113	0.827	0.841	0.900	0.462	0.443	0.461	0.640	0.760	0.979	1.044
Ca	0.010	0.007		0.019	0.005	0.005	0.009	0.003	0.002	0.005	0.004	0.027
Na	0.017	0.011		0.013	0.013	0.020	0.020	0.033	0.011	0.011	0.038	0.013
K	0.936	0.914	0.963	0.955	0.928	0.959	0.928	0.965	0.998	0.917	0.889	0.905
Ba		0.011	0.009				0.002		0.002	0.009	0.003	0.006
F	0.302	0.440	0.192	0.457	0.293	0.161	0.121	0.137	0.400	0.223	0.051	
Fe/Fe + *Mg*	*0.54*	*0.53*	*0.65*	*0.60*	*0.60*	*0.80*	*0.81*	*0.79*	*0.71*	*0.66*	*0.58*	*0.54*

Here and in Tables 3 and 4, *n* = number of analysed grains; FeO* = total Fe calculated as FeO; hyphen = concentration of element below the detection limit.

completely altered to chlorite and leucoxene. Clear parallel orientation of mica flakes and some feldspar phenocrysts defines the gneissic texture of the rock.

Despite the gneissic texture that is characteristic of the SGG, it differs noticeably from the enclosing granitic gneiss that is intruded by SGG. Gneiss is coarsely crystalline, with typical metamorphic granoblastic equigranular or porphyroclastic and augen textures. Commonly a gneissosity or foliation may be observed due to a preferred orientation of tabular plagioclase, lenticular quartz grains, biotite and muscovite flakes.

5. Mineral chemistry

Microprobe analyses were made for all rock-forming minerals of EG, SGG, some pegmatite veins and enclosing schist. A total of 122 mineral grains were analyzed (complete data available from the authors on request). Data on the feldspar compositions are given in the foregoing section. Below, we discuss the compositional features of micas and garnet, on which estimates of magma temperature are based.

Biotite is present in all types of monzogranites. It is of phlogopite–annite composition according to Rieder et al. (1999) classification. It contains 0.5–1.9 wt.% fluorine (Table 2). Biotite from the Wadi Shelomo monzogranite, as compared to that from rocks of the Rehavam pluton, is richer in Fe, Ti, Al, whereas Mg, Mn and F are lower (Table 2; Fig. 3). In the weakly gneissic SGG, biotite is compositionally intermediate between the two varieties of the EG (Fig. 3).

Muscovite is common in the Rehavam and Shahmon plutons (Table 3). Two types of muscovite are distinguished: large euhedral to subhedral flakes (muscovite-1) and small flakes of secondary muscovite unevenly dispersed in feldspar, rarely in biotite (muscovite-2).

In monzogranite from the Rehavam pluton (Mt Rehavam and Wadi Roded areas), a systematic and similar compositional distinction between muscovite-1 and muscovite-2 can be seen. Muscovite-2 contains less Mg, Fe, Ti and more Al (Fig. 4a–c). Morphology of the muscovite-1 flakes, their relationships to other rock-forming minerals, as well as systematic compositional distinction from the secondary muscovite suggest a magmatic origin of the muscovite-1. In weakly gneissic Shahmon monzogranite, compositions of muscovite-1 and muscovite-2 overlap significantly (Table 3; Fig. 4d–f). This suggests that in SGG magmatic muscovite underwent a subsolidus alteration.

Compositions of biotite and garnet from the biotite–garnet schist (country rock for the Wadi Shelomo and Wadi Roded monzogranites) and garnet from pegmatites are reported in Tables 2 and 4. The magmatic origin of garnet in pegmatites and granites from the Wadi Shelomo pluton was justified by Bogoch et al. (1997).

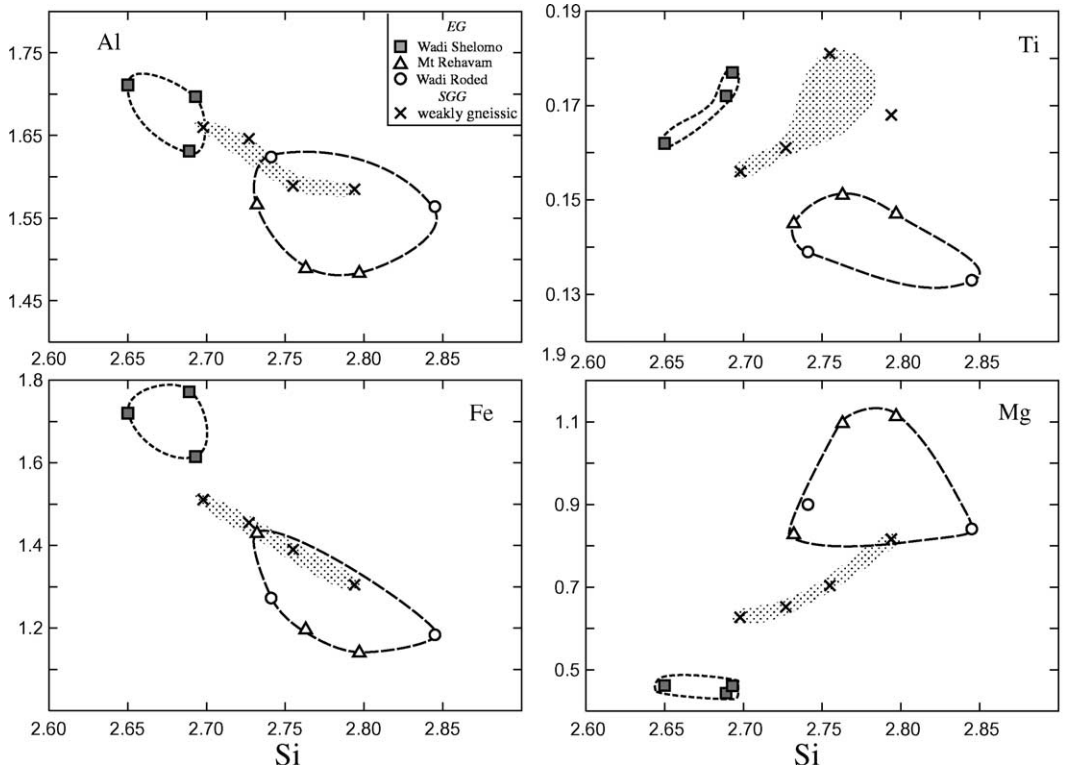

Fig. 3. Biotite compositions plotted on Si vs Al, Ti, Fe and Mg diagrams. Shaded area shows composition of biotite from the SGG.

Table 3
Microprobe analyses of muscovite from the EG and SGG (wt.%)

Sample no.	A39	A38	A102	A101	A39	A38	A102	A101	A41	A48	A41	A99	A57	A89-1	A50	A89	A57	A89-1	A50
Pluton	Rehavam (Mt Rehavam area)								Rehavam (Wadi Roded area)			Shahmon							
	Muscovite-1				Muscovite-2				Muscovite-1		Muscovite-2	Muscovite-1					Muscovite-2		
n	1	1	2	1	1	1	1	1	2	1	3	1	1	1	1	2	2	1	1
SiO_2	45.07	45.06	45.26	44.78	45.24	44.46	45.64	47.35	46.77	46.45	47.64	45.93	46.17	46.82	45.85	45.87	45.41	46.36	46.12
TiO_2	0.85	1.03	1.10	1.06	-	0.08	0.32	0.00	0.85	0.72	0.18	0.77	1.09	1.24	0.97	0.87	0.14	-	-
Al_2O_3	31.43	30.09	30.55	30.43	32.36	33.03	32.48	31.31	32.70	32.90	34.61	34.61	31.43	32.53	32.19	32.82	31.88	34.56	32.43
FeO*	4.64	5.27	4.97	5.44	4.59	4.05	4.09	3.97	3.48	2.95	2.37	2.69	4.39	4.66	4.08	3.75	4.41	3.18	4.01
MnO	-	0.08	0.09	0.10	-	0.07	0.07	0.09	0.14	0.07	0.06	-	0.07	0.06	-	0.09	0.04	0.09	0.06
MgO	1.15	1.48	1.46	1.51	1.07	0.77	1.09	0.90	1.24	1.30	0.90	0.98	1.22	1.07	1.05	1.05	0.96	0.74	1.12
Na_2O	0.33	0.28	0.40	0.38	0.39	0.39	0.43	1.75	0.34	0.33	0.27	0.52	0.40	0.16	0.37	0.39	0.28	0.39	0.31
K_2O	11.01	11.19	10.90	10.81	10.78	11.07	10.95	9.98	10.65	10.89	10.62	10.64	10.73	7.43	10.03	10.51	10.92	9.48	10.82
BaO	-	0.07	0.03	-	0.09	0.12	0.08	0.25	0.00	0.09	0.02	0.05	0.10	-	0.12	0.09	0.20	0.20	0.17
F	0.58	0.58	0.82	0.47	0.59	0.39	0.63	0.76	0.97	0.63	0.41	0.69	0.64	0.69	1.41	0.52	0.78	0.51	0.54
	95.06	95.12	95.57	94.98	95.11	94.42	95.78	96.36	97.14	96.31	97.08	96.88	96.23	94.66	96.07	95.97	95.01	95.50	95.57
O=F	0.24	0.24	0.34	0.20	0.25	0.17	0.26	0.32	0.44	0.27	0.19	0.29	0.27	0.29	0.59	0.22	0.33	0.21	0.23
Total	94.82	94.88	95.23	94.78	94.86	94.26	95.52	96.04	96.70	96.05	96.88	96.59	95.96	94.37	95.48	95.75	94.69	95.29	95.34
	Atoms to 11 oxygens																		
Si	3.100	3.118	3.113	3.096	3.102	3.066	3.105	3.194	3.125	3.117	3.134	3.058	3.128	3.151	3.114	3.096	3.124	3.106	3.133
Al^{iv}	0.900	0.882	0.887	0.904	0.898	0.934	0.895	0.806	0.875	0.883	0.866	0.942	0.872	0.849	0.886	0.905	0.877	0.894	0.867
Al^{vi}	1.648	1.572	1.590	1.576	1.717	1.751	1.708	1.684	1.700	1.720	1.817	1.774	1.638	1.731	1.691	1.706	1.708	1.835	1.729
Ti^{vi}	0.044	0.054	0.057	0.055	0.000	0.004	0.017	0.000	0.043	0.036	0.009	0.039	0.055	0.063	0.050	0.044	0.008	0.000	0.000
Fe	0.267	0.305	0.286	0.314	0.263	0.234	0.233	0.224	0.194	0.165	0.130	0.149	0.249	0.262	0.232	0.212	0.254	0.178	0.228
Mn	0.000	0.004	0.005	0.006	0.000	0.004	0.004	0.005	0.008	0.004	0.004	0.000	0.004	0.003	0.000	0.005	0.003	0.005	0.003
Mg	0.118	0.153	0.150	0.156	0.110	0.079	0.110	0.090	0.124	0.130	0.088	0.098	0.124	0.107	0.107	0.106	0.099	0.074	0.113
Na	0.044	0.037	0.053	0.051	0.052	0.052	0.057	0.229	0.045	0.042	0.035	0.067	0.052	0.021	0.048	0.052	0.038	0.051	0.040
K	0.966	0.988	0.956	0.953	0.943	0.974	0.950	0.859	0.908	0.932	0.892	0.903	0.927	0.638	0.869	0.905	0.958	0.810	0.938
Ba	0.000	0.002	0.001	0.000	0.002	0.003	0.002	0.007	0.000	0.002	0.001	0.001	0.003	0.000	0.003	0.003	0.005	0.005	0.005
F	0.126	0.128	0.179	0.104	0.127	0.086	0.134	0.163	0.205	0.134	0.056	0.146	0.137	0.147	0.302	0.111	0.170	0.108	0.115
Mg/Mg + Fe	*0.31*	*0.33*	*0.34*	*0.33*	*0.29*	*0.25*	*0.32*	*0.29*	*0.39*	*0.44*	*0.40*	*0.40*	*0.33*	*0.29*	*0.32*	*0.33*	*0.28*	*0.29*	*0.33*

Shahmon pluton samples are from weakly gneissic granites, except A89 (gneissic granite).

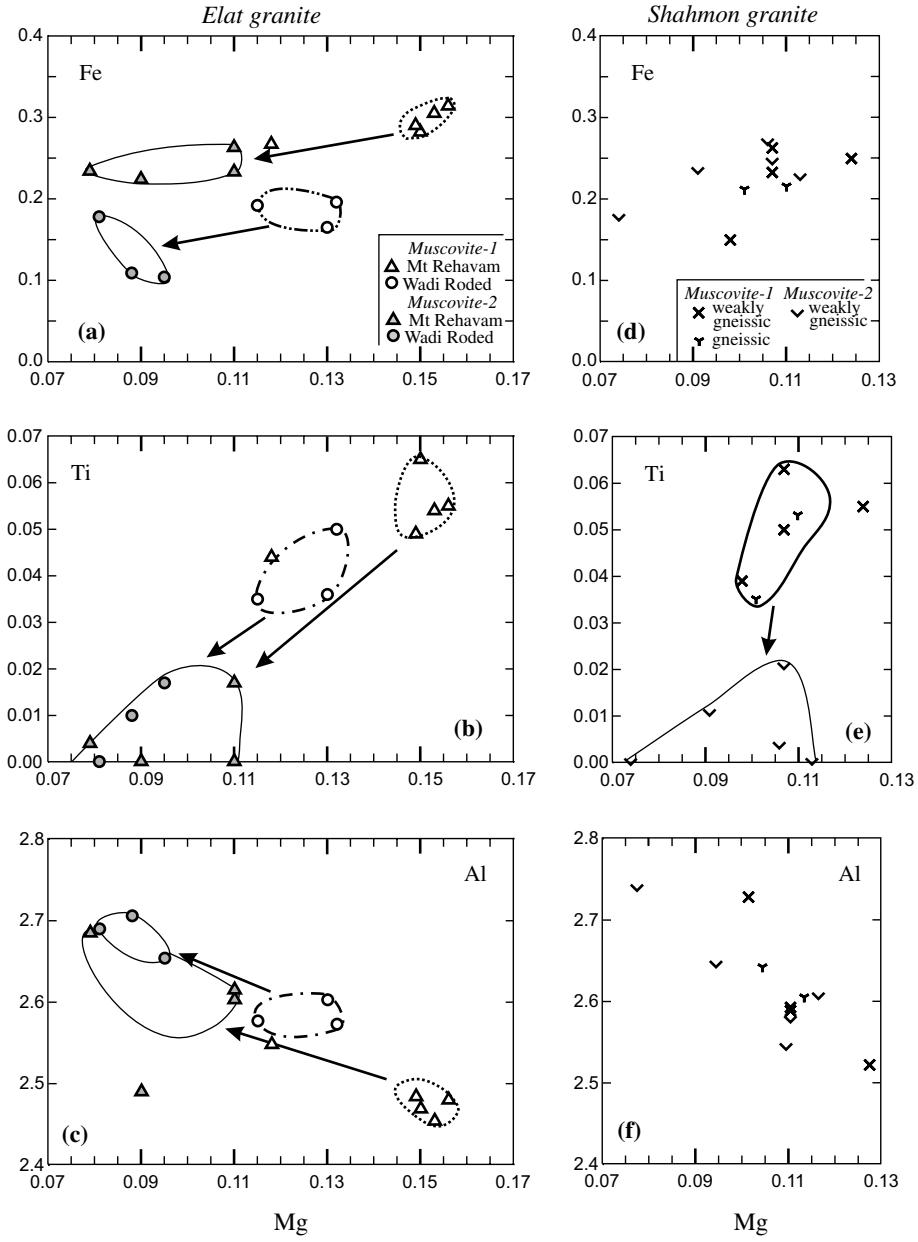

Fig. 4. Compositions of muscovite-1 and muscovite-2 in the EG and SGG plotted on Mg vs Fe, Ti and Al diagrams. Minerals were studied in the same rock samples (see Table 3). Arrows point to compositional distinctions between muscovite-1 and muscovite-2.

The distinctions in chemical compositions of the minerals from magmatic and metamorphic rocks are significant. Biotite in schist is richer in Mg and contains less fluorine than in granites, and garnet is almandine with a higher proportion of pyrope (13.7–18.3%) and low Mn as compared to garnet from pegmatites (Tables 2 and 4).

6. Geochemistry

Data for chemical compositions of representative samples are reported in Tables 5 and 6. Both EG and SGG have a restricted silica range, with SiO_2 contents of 72.5–75.5%. In most samples, except from the Wadi Shelomo pluton, Na_2O/K_2O ratio ~1.25–1.5, and Zr concentration is comparatively low, from 60 to 100 ppm. EG and SGG samples have high (13.0–15.3%) Al_2O_3. The aluminium saturation index value (*ASI*) ranging from 1.03 to 1.16, and the presence of 1.1–1.9 wt.% of normative corundum, indicate that the granites are peraluminous (Fig. 5A; Table 5). In terms of their SiO_2–K_2O relationship, EG and SGG samples plot in the lower part of the calc-alkaline, high-K field (Fig. 5B).

Within the EG type, monzogranites from the Wadi Shelomo and Rehavam plutons are noticeably distinct.

Table 4
Representative microprobe analyses of garnet from the enclosing biotite-garnet schists and pegmatites (wt.%)

Sample no.	A 34	A 107-1	A26	A3-1	A107	A97
Rock	Schist		Pegmatite			
n	1	2	1	1	2	1
SiO_2	37.14	37.79	36.29	35.77	36.38	36.22
TiO_2	-	0.07	0.07	0.52	-	-
Al_2O_3	20.81	20.62	19.73	20.15	20.82	20.33
FeO*	34.82	34.74	24.07	31.8	26.64	21.38
MnO	2.67	1.90	17.97	10.43	15.05	21.74
MgO	3.36	4.50	0.44	0.61	0.63	0.15
CaO	1.55	0.83	0.71	1.15	0.21	0.33
Total	100.35	100.43	99.28	100.43	99.73	100.15
FeO-calc	33.08	33.00	22.87	30.21	25.31	20.31
Fe_2O_3-calc	1.93	1.93	1.34	1.77	1.48	1.19
Total-calc	100.46	100.48	99.33	100.61	99.74	100.23
			Atoms to 12 oxygens			
Si	2.980	3.012	3.013	2.936	2.998	2.986
Al^{iv}	0.02			0.064	0.009	0.014
Al^{vi}	1.947	1.935	1.929	1.884	2.012	1.960
Fe^{3+}	0.117	0.116	0.083	0.109	0.092	0.074
Ti		0.004	0.004	0.032	0.000	
Fe^{2+}	2.220	2.200	1.588	2.074	1.744	1.400
Mg	0.402	0.535	0.054	0.075	0.078	0.018
Mn	0.181	0.128	1.264	0.725	1.051	1.518
Ca	0.133	0.071	0.063	0.101	0.019	0.029
			End members, mol%			
Alm	75.6	74.9	53.3	61.1	60.4	47.2
And	4.5	2.4	2.1	4.4	0.6	1.0
Pyr	13.7	18.3	1.8	3.2	2.7	0.6
Spess	6.2	4.4	42.7	31.3	36.3	51.2

Wadi Shelomo area: samples A34, A26 and A3-1; Wadi Roded area: A107-1 and A107; Shahmon pluton: A97. Ferrous and ferric iron recalculated after Knowles (1987); End members (mol%) are determined according to Rickwood (1968).

Monzogranite in Wadi Shelomo is richer in SiO_2, FeO*, K_2O, Ba, Zr, Th, LREE and contains less MgO, Na_2O, Sr and HREE (Tables 5 and 6; Figs. 6 and 7A). The Eu/Eu* values are lower than in the Mt Rehavam area (0.44 and 0.55 vs 0.75 and 0.92).

SGG is chemically similar to monzogranite from the Rehavam pluton, although it is slightly richer in Ba and Zr and poorer in HREE (Figs. 6 and 7B). Weakly gneissic and gneissic Shahmon monzogranites are not distinguished in major and trace element content (Fig. 6). Data from Tables 5 and 7 and Fig. 8 illustrate that the SGG differs significantly from the enclosing Elat granitic gneiss in SiO_2, Al_2O_3, Na_2O, K_2O, Sr, Y and REE abundance. Thus, the whole-rock chemistry, which is in good agreement with petrographic studies, indicates that Elat granitic gneiss cannot be considered as part of SGG.

7. Rb–Sr isotope data

Rb-Sr isotope study was performed on 7 whole-rock samples, 5 garnet and 6 muscovite separations. However, it turned out that Sr contents of all garnet and 4 muscovite separations are near or below the detection limit ($\leqslant$2 ppm). Trustworthy data have been obtained only on two muscovite and six whole-rock samples (Table 8).

Isotope measurements in one muscovite and three whole rock samples from the Wadi Shelomo pluton form an isochron yielding date of 623 ± 24 Ma, with I_{Sr} = 0.7071 ± 0.0099 and MSWD = 3.5 (Fig. 9a). Similar date of 621 ± 12 Ma, with I_{Sr} = 0.7067 ± 0.0075 is obtained from the whole rock and muscovite samples collected from a pegmatite vein (Fig. 9b). Three whole rock samples also yielded date of about 630 Ma, but with the error more than 100 My. The EG is homogeneous, unfoliated and its magmatic texture is well preserved. Thus it is likely that the Rb–Sr date indicates the time of emplacement, although high value of age-error does not allow to constrain this time properly.

In the Shahmon pluton, four points (3 whole rock samples and 1 muscovite) form an isochron yielding date of 640 ± 9 Ma, with I_{Sr} = 0.7039 ± 0.0003 and MSWD = 1.01 (Fig. 9c). An isochron calculated only for whole rock samples gave a similar but less precise date of 645 ± 14 Ma; I_{Sr} = 0.7038 ± 0.0003; MSWD = 1.1 (Fig. 9d). This suggests that the date of 640 ± 9 Ma

Table 5
Chemical composition of representative EG and SGG samples, major (wt.%) and selected trace elements (ppm)

Pluton	Rehavam, EG							Wadi Shelomo, EG						Shahmon, SGG								
Sample no.	A38	A102	A101	A39	A41	A48	A44	A6	A29	A24	A4	A9	A33	A57	A99	A58	A50	A89-1	A114	A89	A112a-1	A112-a
	1	2	3	4	5	6	7	8	9	10	11	12	13	14	15	16	17	18	19	20	21	22
SiO_2	72.5	72.80	73.00	73.70	73.40	73.80	74.00	74.00	74.70	75.00	75.40	75.40	75.50	73.20	73.20	73.40	73.50	73.60	72.90	73.00	73.10	73.30
TiO_2	0.13	0.14	0.13	0.15	0.10	0.12	0.13	0.14	0.15	0.17	0.15	0.17	0.15	0.17	0.14	0.15	0.15	0.14	0.17	0.14	0.16	0.15
Al_2O_3	15.3	14.50	15.00	14.40	14.80	14.90	15.00	13.40	13.50	13.00	13.40	13.30	13.20	14.60	14.70	14.40	14.20	14.50	15.00	14.70	14.80	14.80
Fe_2O_3	0.18	0.73	0.57	0.68	0.74	0.49	0.12	1.13	0.76	1.04	0.30	0.18	0.35	0.81	0.28	0.90	0.72	0.70	0.56	0.25	0.33	0.19
FeO	0.80	0.43	0.39	0.44	0.30	0.52	0.91	0.56	0.84	0.64	1.24	1.56	1.16	0.40	0.71	0.24	0.48	0.16	0.55	0.47	0.59	0.67
MnO	0.04	0.04	0.03	0.04	0.04	0.02	0.04	0.03	0.03	0.03	0.03	0.04	0.03	0.02	0.02	0.04	0.03	0.02	0.02	0.02	0.02	0.02
MgO	0.28	0.52	0.46	0.32	0.20	0.23	0.26	0.19	0.21	0.14	0.19	0.16	0.19	0.27	0.29	0.23	0.27	0.27	0.37	0.29	0.34	0.29
CaO	1.21	0.78	0.78	1.10	0.73	1.02	1.15	0.68	0.48	1.00	1.18	0.62	1.00	0.76	1.02	0.90	1.19	0.86	0.88	1.08	1.02	0.88
Na_2O	4.53	5.2	5.12	4.68	4.81	4.89	4.78	4.00	4.30	3.80	3.82	3.87	3.83	4.82	4.96	4.62	4.80	4.90	4.92	4.70	4.86	4.81
K_2O	4.45	3.34	3.71	3.45	3.61	3.49	3.25	4.03	3.77	4.08	3.76	3.64	3.62	3.50	3.54	3.62	3.50	3.50	3.47	3.76	3.20	3.25
P_2O_5	0.06	0.06	0.06	0.05	0.05	0.05	0.04	0.07	0.04	0.05	0.05	0.05	0.04	0.05	0.05	0.05	0.05	0.05	0.08	0.06	0.05	0.06
LOI	0.89	0.88	0.74	0.65	0.50	0.41	0.51	1.06	1.19	0.67	0.73	1.07	0.82	0.74	1.27	0.82	0.75	0.82	1.06	1.05	1.06	1.07
Total	100.4	99.42	99.99	99.66	99.28	99.94	100.19	99.29	99.97	99.62	100.25	100.06	99.89	99.34	100.18	99.37	99.64	99.52	99.98	99.52	99.53	99.49
Rb	100	93	100	80	120	80	84	105	110	82	105	105	93	78	105	83	77	80	72	90	70	70
Ba	800	450	590	500	360	500	500	650	550	700	600	610	700	650	720	720	740	690	680	600	680	740
Sr	450	360	340	390	200	400	390	100	92	115	98	100	90	390	360	410	420	380	400	370	470	460
Zr	67	70	70	70	57	68	70	110	120	120	100	110	110	90	92	100	93	80	93	74	97	87
Nb	7	8	6	6	12	8	9	10	10	8	10	8	8	8	5	6	8	5	4	4	5	5
Y	9	12	8	8	10	6	11	11	8	17	8	11	15	5	11	4	6	7	7	8	10	5
ASI	1.06	1.07	1.08	1.07	1.13	1.09	1.11	1.10	1.12	1.04	1.07	1.16	1.10	1.11	1.06	1.10	1.03	1.08	1.12	1.07	1.11	1.14
AI	0.80	0.84	0.83	0.79	0.80	0.79	0.76	0.82	0.83	0.82	0.77	0.77	0.77	0.80	0.82	0.80	0.82	0.82	0.79	0.80	0.77	0.77
Na_2O/K_2O	1.02	1.56	1.38	1.36	1.33	1.40	1.47	0.99	1.14	0.93	1.02	1.06	1.06	1.38	1.40	1.28	1.37	1.40	1.42	1.25	1.52	1.48
C	1.39	1.07	1.3	1.1	1.79	1.35	1.63	1.41	1.59	0.64	1.03	2.01	1.27	1.64	0.98	1.38	0.48	1.22	1.76	1.1	1.63	1.94

Areas of the Rehavam pluton: Mt Rehavam (1–4) and Wadi Roded (5–7). Shahmon pluton rocks: weakly gneissic (14–18) and gneissic (19–22) granite. *ASI* = $Al_2O_3/(CaO + Na_2O + K_2O)$, mol%; *AI* = $(Na_2O + K_2O)/Al_2O_3$, mol%; C = CIPW-normative corundum, wt.%.

Table 6
REE and selected trace element content in the EG and SGG, ppm

Pluton	Rehavam, EG		Wadi Shelomo, EG		Shahmon, SGG	
Sample no.	A38	A102	A29	A4	A50	A89-1
Hf	2.5	2.2	2.7	1.9	3.0	1.0
Ta	4.2	3.2	2.8	2.3	3.9	3.1
Th	4.5	4.4	8.8	7.1	5.9	4.3
U	0.9	4.1	1.3	1.0	1.9	1.0
Ga	22.8	21.2	20.8	18.1	21.2	22.1
V	38	12	25	5	14	6
Cu	5	5	2	6	4	2
Pb	22	15	14	14	18	17
Zn	35	41	41	34	45	29
Sc	2.7	1.9	3.9	3.1	2.7	1.6
Cs	3.3	4.1	2.7	2.7	3.1	2.3
La	13.04	12.81	24.25	22.11	19.39	11.89
Ce	27.64	27.76	49.77	44.81	37.67	34.91
Pr	3.19	3.16	5.56	4.96	4.48	2.95
Nd	11.84	11.52	20.12	17.17	15.94	10.44
Sm	2.39	2.38	3.70	3.04	2.62	1.97
Eu	0.67	0.56	0.50	0.52	0.68	0.58
Gd	2.01	2.13	3.08	2.53	1.89	1.52
Tb	0.31	0.34	0.42	0.34	0.26	0.22
Dy	1.77	2.14	1.89	1.52	1.36	1.20
Ho	0.37	0.46	0.30	0.24	0.27	0.22
Er	0.99	1.17	0.73	0.61	0.74	0.61
Tm	0.15	0.18	0.09	0.08	0.11	0.09
Yb	1.06	1.19	0.63	0.54	0.69	0.64
Lu	0.16	0.17	0.11	0.09	0.10	0.09
Eu/Eu*	0.92	0.75	0.44	0.55	0.89	0.98
La_n/Yb_n	8.86	7.70	27.61	29.43	20.07	13.27

Samples A50 and A89-1 = weakly gneissic granite.

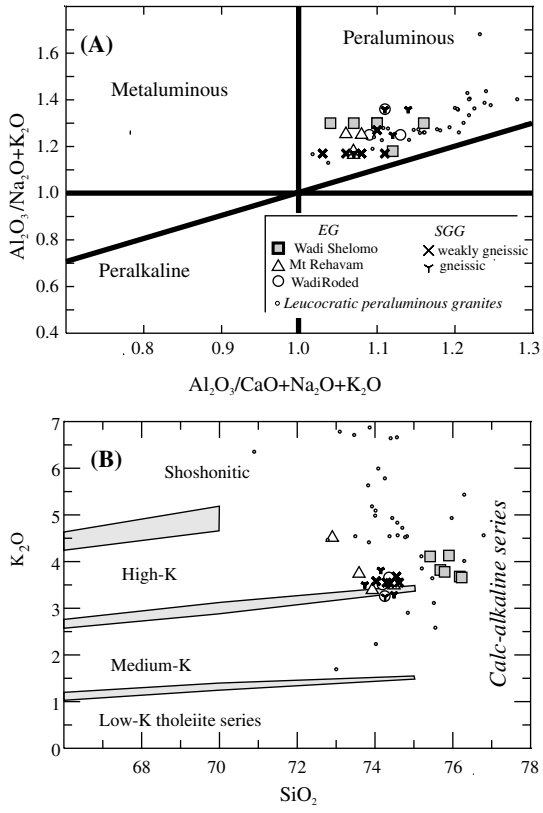

Fig. 5. Location of the EG and SGG compositions in the classification diagrams. A = $Al_2O_3/CaO + Na_2O + K_2O$ vs $Al_2O_3/Na_2O + K_2O$ (from Maniar and Piccoli, 1989); B = SiO_2 vs K_2O (the shaded bands are the fields that define the boundary between series (Rickwood, 1989). Sources of data on leucocratic peraluminous granite compositions are from Le Fort (1981); Nabelek et al. (1992); Inger and Harris (1993)).

for weakly gneissic monzogranite is a reliable estimate. Its geological meanings envisioned below, in the "Discussion".

8. Oxygen isotope ratios

The oxygen isotope analyses of quartz, zircon and garnet are given in Table 9. The $\delta^{18}O$ (Qtz) values of EG in Wadi Shelomo pluton range from 10.09‰ to 10.38‰; in the Rehavam area these values are higher, 10.71–11.17‰. Difference in isotope ratios could be caused by differences in the depth of sampling. Samples collected in the Wadi Shelomo pluton characterize its uppermost part, whereas samples from the Rehavam area represent deeper levels. It is known that in slowly cooled plutonic rocks the isotope ratio of quartz would reset simply by closed system oxygen exchange with fast-diffusing phases like feldspar and mica down to its closure temperature (Valley, 2001). Considering that cooling rate in the uppermost part of the pluton are bound to be higher than in the deeper one, closure temperature for oxygen diffusion in quartz (~600 °C) would be attained faster in the Wadi Shelomo pluton and isotope ratios of quartz would reset by a smaller amount. This suggests that the $\delta^{18}O$ (Qtz) values of 10.25‰ ± 0.12‰ obtained in EG samples from the Wadi Shelomo pluton could be close to magmatic values. Data on $\delta^{18}O$ values of quartz and zircon in sample YE-33 strongly support this assumption (Table 9). Zircon is capable to retain magmatic oxygen isotope ratios through slow cooling and hydrothermal events (Valley et al., 1994; Peck et al., 2000), so the $\delta^{18}O$ (Zrn) value is considered as magmatic. Calculated model granitic rock compositions have equilibrium $\Delta^{18}O$ (WR-Zrn) values of ~2‰ (Valley et al., 1994) and $\Delta^{18}O$ (Qtz-WR) values of ~1‰ (Wickham et al., 1996). In the sample YE-33 the $\delta^{18}O$ (Zrn) value is 6.97‰, the $\delta^{18}O$ (Qtz) value is 10.31 ‰. In accordance with the above data on whole-rock-zircon and whole-rock-quartz fractionation, the estimated $\delta^{18}O$ (WR) value proved to be the same, ~9‰.

Quartz–zircon and quartz–garnet oxygen isotope fractionations can help interpret the crystallization and cooling history of Wadi Shelomo pluton. Since closure temperatures for diffusion of oxygen in zircon and quartz are different (~800 °C and 600 °C, respectively), interpretation of quartz-zircon fractionations should

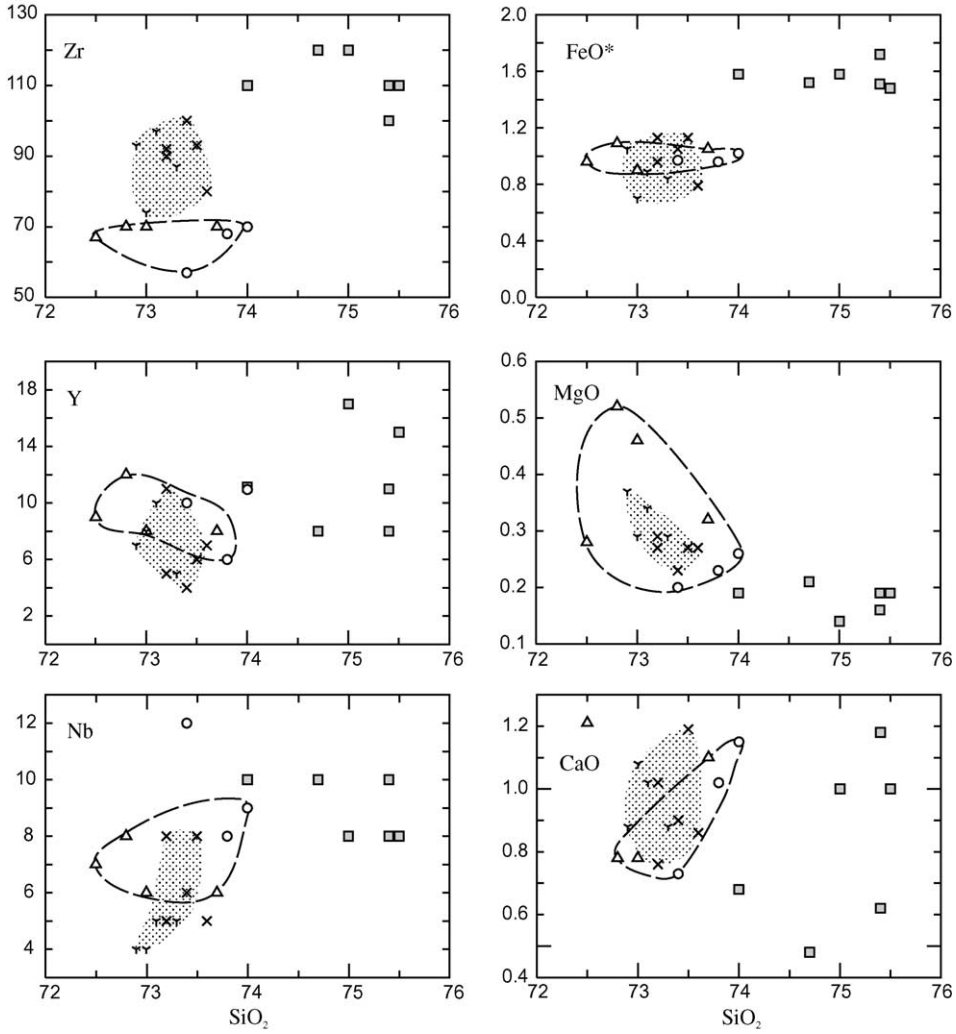

Fig. 6. Silica variation diagrams for selected major and trace elements in the EG and SGG.

take into account the reset of $\delta^{18}O$ (qtz) by closed system cooling. Based on the Fast Grain Boundary model (Eiler et al., 1992) the $\Delta^{18}O$ (Qtz–Zrn) = 3.34‰ in sample YE-33 implies cooling of 60 °C/Ma for the Wadi Shelomo pluton. Despite the expected zero fractionation between zircon and garnet, the $\Delta^{18}O$ (Qtz–Zrn) = 3.34‰ in YE-33 is significantly lower than the average value of $\Delta^{18}O$ (Qtz–Grt) = 3.67‰ in the three other analyzed samples. Given the relatively homogenous $\delta^{18}O$ (qtz) value of Wadi Shelomo pluton, 10.25 ± 0.12‰, and assuming that quartz was reset by the same amount in the four analyzed rocks, the above difference might suggest that garnet crystallized at lower temperatures and later stages than zircon. Its increased abundance in pegmatites and aplites supports this interpretation.

The $\delta^{18}O$ (Qtz) value of Shahmon gneissic granite, 11.27 ± 0.05‰, is considerably higher than in EG. This value may represent recrystallization of quartz and its re-equilibration at metamorphic temperatures.

9. Discussion

9.1. The peraluminous composition of EG and SGG

Both EG and SGG are peraluminous, with the *ASI* ranging from 1.03 to 1.16 (Table 5, Fig. 5A). Generally three main groups of peraluminous granites are distinguished (Patiño Douce, 1999): peraluminous leucocratic granites, strongly peraluminous S-type, and Cordilleran peraluminous two-mica granites. Compositional fields of these groups are shown in Fig. 10. All SGG and most EG samples plot within the field of peraluminous leucocratic granites. Peraluminous leucocratic granite commonly make up relatively small post-collision plutons (Le Fort, 1981 and references therein; Nabelek et al., 1992; Inger and Harris, 1993). They include two-mica and muscovite-garnet granites and do not contain low-pressure, high-temperature mafic aluminous minerals (e.g., cordierite) and aluminosilicates, which are characteristic of strongly peraluminous S-type granites

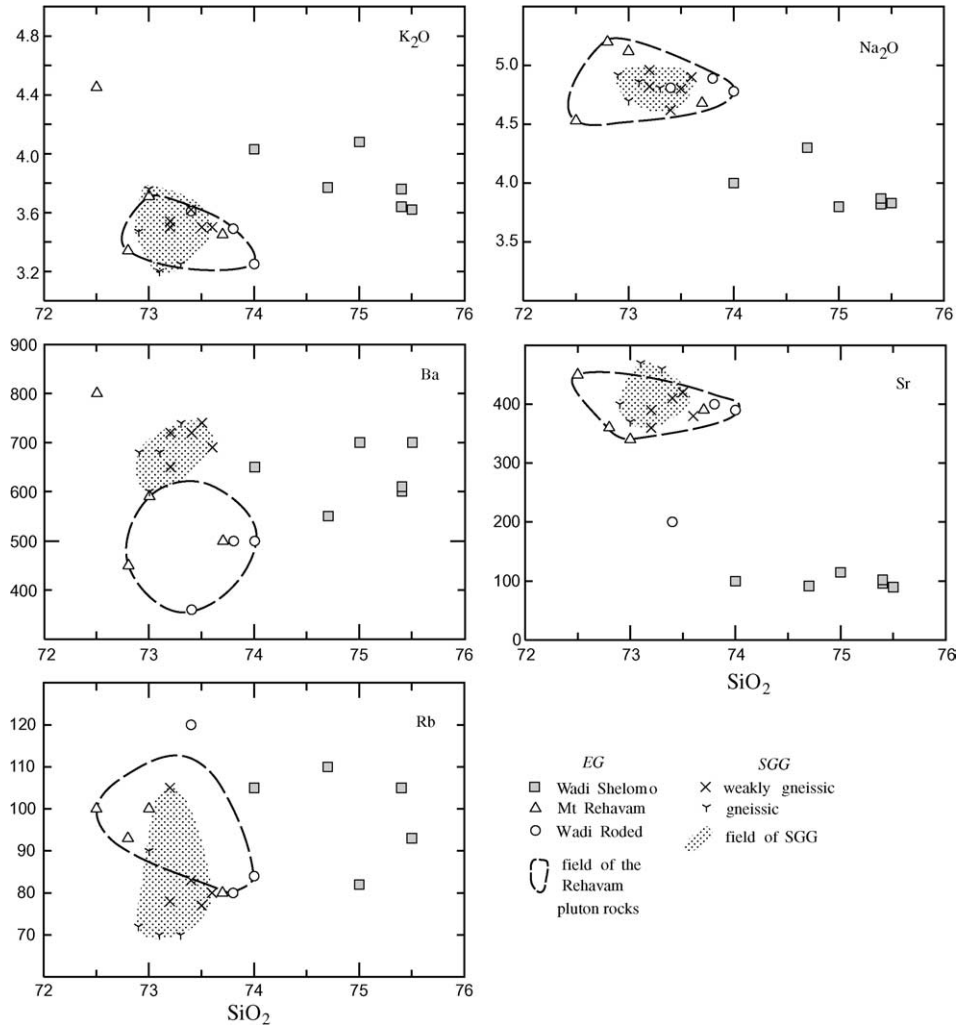

Fig. 6 (*continued*)

(Chappell and White, 1974). Almost all peraluminous leucogranites from typical plutons are high-K and calc-alkaline (Fig. 5B). Comparison of EG with typical peraluminous leucocratic granites demonstrate significant similarity in geological, mineralogical and chemical characteristics, so that EG can be classified as peraluminous leucocratic granite. Since chemical features of the SGG are almost the same as those of EG in the Rehavam pluton of EG (Fig. 6), it also should be considered as peraluminous leucocratic granite.

9.2. Estimation of magma temperature

To obtain a direct estimation of magma temperature, we looked for melt inclusions in the quartz grains from the EG. However, only secondary fluid inclusions were found, so the muscovite–biotite geothermometer (Hoisch, 1989) was used to assess magma temperature. The muscovite–biotite assemblage is abundant in three areas: Mt Rehavam, Wadi Roded and Shahmon. However, it was shown above that in the Shahmon pluton the magmatic muscovite was altered. For this reason, assessment of temperature was performed for the Wadi Roded and Mt Rehavam granites only. Calculations were carried out for 2 and 4 kbar, assuming that these pressures embrace the more likely depth of the plutons emplacement. Temperature estimates of ~760–800 °C were obtained for the Mt Rehavam pluton and ~680–740 °C for the Wadi Roded rocks (Table 10). Higher crystallization temperatures in monzogranite of the Mt Rehavam area are in good agreement with the field data on deeper level of the pluton exposure (Section 2).

Temperatures in the contact zones of the Shelomo and Rehavam (Wadi Roded) plutons were estimated based on biotite-garnet geothermometery in the enclosing schist immediately near the contact with monzogranite (Bhattacharya et al., 1992; Kleemann and Reinhardt, 1994). It follows from Table 10 that metamorphic assemblages were formed in the range of ~620–650 °C. These values are similar to the temperatures of regional metamorphism in the same areas (Matthews et al., 1989; Katz et al., 1998; Cosca et al., 1999). Taking into account that

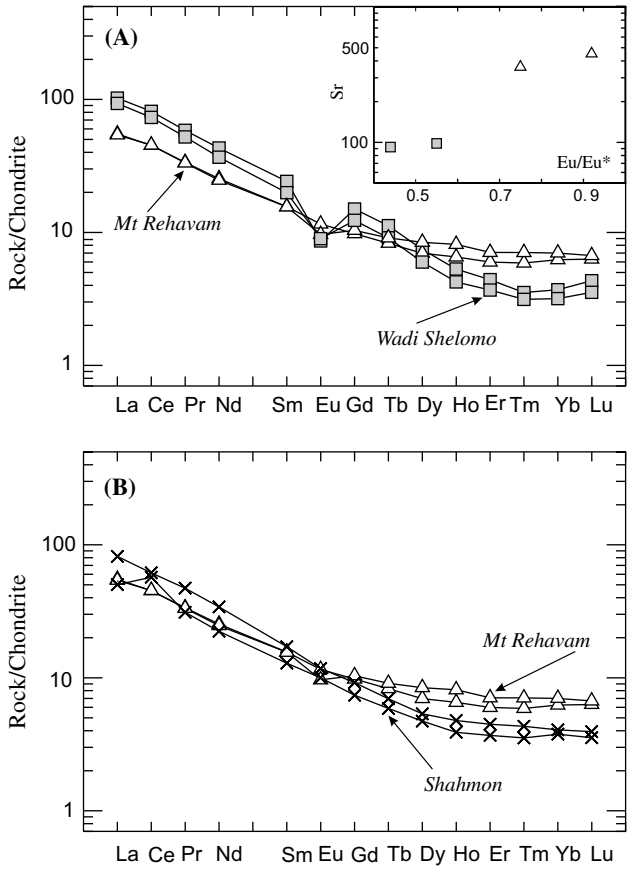

Fig. 7. Chondrite normalized REE patterns of the EG (Mt Rehavam and Wadi Shelomo areas) and SGG. In the Inset, Eu/Eu* vs Sr diagram.

temperature in the inner part of the Wadi Roded granite was estimated at 680–740 °C, temperature decrease of $\geqslant$30 °C should have occurred near the granite contact. Judging from the abundance of pegmatites and from the dominant pegmatitic texture of granite next to the metamorphic country rocks, decrease of temperature of magma crystallization could have been caused by enrichment of the outer zone of the pluton in water-rich fluids. Experimental data (Johannes and Holtz, 1996; Holtz et al., 2001) indicate that the solidus temperature of water-rich magma is ~650 °C at pressures of 3–5 kbar, which compares well with that estimated for the country rocks near the contact.

9.3. Relations between the granites from Wadi Shelomo and Rehavam plutons

Although the Wadi Shelomo and Rehavam plutons are made up of the same Elat type monzogranites, a number of distinctions in rock composition are clearly exhibited. The monzogranite from Wadi Shelomo contains less plagioclase and more quartz (Table 1; Fig. 2); muscovite is absent, but garnet is common. Biotite from the Wadi Shelomo granite is richer in Al, Fe, Ti and poorer in Si and Mg (Fig. 4). Differences in whole-rock chemical composition are also rather systematic. The Wadi Shelomo monzogranite is richer in SiO_2, FeO*, K_2O, Ba and Zr, whereas MgO, Na_2O and Sr are lower as compared to samples from the Rehavam pluton (Table 5; Fig. 6). Monzogranite from Wadi Shelomo is richer in LREE and contains less HREE, La_n/Yb_n ratios are 27.5 and 29.2 vs 7.7 and 8.8 (Fig. 8; Table 6). The negative Eu anomaly is much more pronounced: Eu/Eu* values are 0.44 and 0.55, whereas in the Rehavam pluton these values are 0.75 and 0.92 (Table 6; Fig. 8). It is illustrated in the Eu/Eu* vs Sr plot (Inset in Fig. 7A) that decrease of Eu/Eu* value is accompanied by Sr decrease. All these distinctions suggest that the silicic magma of the Wadi Shelomo pluton could have been produced by fractional crystallization of the less evolved magma of the Rehavam monzogranite. The REE abundance and correlation between

Table 7
Chemical composition of the enclosing Elat granitic gneiss (wt.%, ppm)

Sample no.	A124	A122	YE9	YE16	ET92	ET2	ET93
	1	2	3	4	5	6	7
SiO_2	74.2	75.1	74.6	75.9	75.7	73	75.2
TiO_2	0.16	0.17	0.15	0.16	0.26	0.16	0.19
Al_2O_3	13.25	13.25	13.25	12.45	12.7	12.3	12.4
Fe_2O_3*	1.63	1.57	1.8	1.49	2.51	1.38	1.81
MnO	0.03	0.05	0.04	0.02	-	-	-
MgO	0.35	0.31	0.29	0.19	0.3	0.16	0.31
CaO	0.88	1.02	0.93	0.92	0.73	0.62	0.74
Na_2O	3.79	3.91	4.08	4	3.36	3.36	3.47
K_2O	4.36	3.86	3.85	3.74	4.59	5.33	4.64
P_2O_5	0.05	0.05	0.05	0.03	0.03	0.05	0.03
LOI	0.76	0.52	0.55	0.8	0.74	0.67	0.7
Total	99.45	99.8	99.52	99.62	100.92	97.03	99.5
Rb	96	10	100	55	55	73	61
Ba	840	700	700	250	348	394	321
Sr	120	115	120	83	58	34	52
Zr	120	120	120	240	308	207	204
Nb	10	9	9	7	9	4	6
Y	15	20	27	41	27	24	39
La	n.d.	n.d.	n.d.	66	16.2	80.4	n.d.
Ce	n.d.	n.d.	n.d.	158	38	175	n.d.
Pr	n.d.	n.d.	n.d.	16.6	4.92	17.7	n.d.
Nd	n.d.	n.d.	n.d.	62	19.5	68.3	n.d.
Sm	n.d.	n.d.	n.d.	11.3	5.06	12.6	n.d.
Eu	n.d.	n.d.	n.d.	0.27	0.23	0.43	n.d.
Gd	n.d.	n.d.	n.d.	11.74	4.67	9.71	n.d.
Tb	n.d.	n.d.	n.d.	1.43	0.72	1.19	n.d.
Dy	n.d.	n.d.	n.d.	7.72	5.09	6.1	n.d.
Ho	n.d.	n.d.	n.d.	1.5	1.11	1.21	n.d.
Er	n.d.	n.d.	n.d.	4.62	3.33	3.23	n.d.
Tm	n.d.	n.d.	n.d.	0.71	0.57	0.51	n.d.
Yb	n.d.	n.d.	n.d.	4.42	3.62	3.44	n.d.
Lu	n.d.	n.d.	n.d.	0.63	0.58	0.51	n.d.
Eu/Eu*	n.d.	n.d.	n.d.	0.07	0.14	0.11	n.d.

1–3 = SW of Wadi Shahmon; 4–7 = the Mt Shahmon area (5–7, after Kessel, 1995). Fe_2O_3* = total Fe as Fe_2O_3; n.d. = not determined; hyphen = concentration of element below the detection limit.

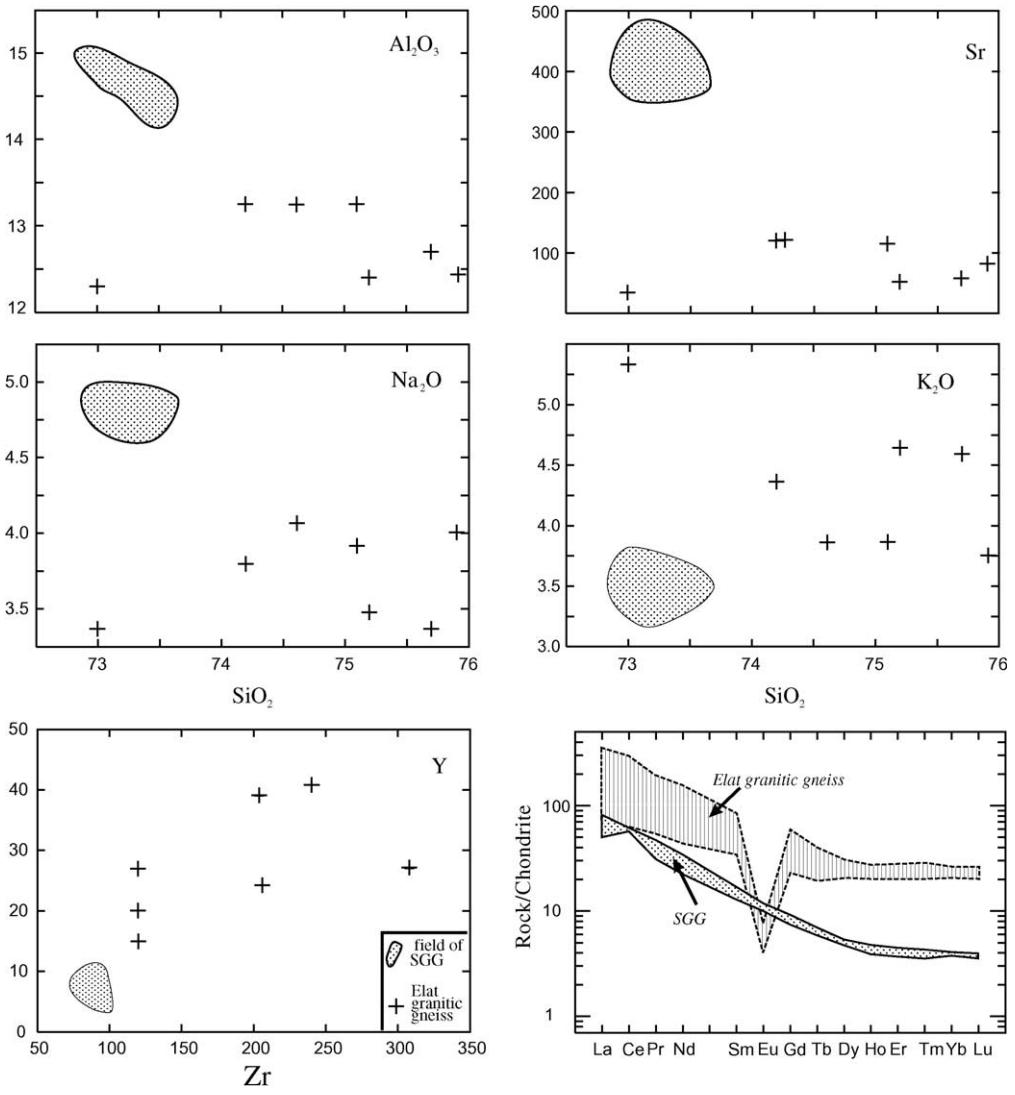

Fig. 8. Comparison of chemical compositions of the SGG and Elat granitic gneiss.

Table 8
Rb-Sr isotope data for the EG and SGG

Sample no.	Rock type	Rock/min.	Rb (ppm)	Sr (ppm)	$^{87}Rb/^{86}Sr$	$^{87}Sr/^{86}Sr$
Wadi Shelomo pluton						
A4	Monzogranite	WR	110.2	104	3.075	0.73240
A26	Pegmatite	WR	197.2	27.0	21.53	0.90242
A3-1	Pegmatite	WR	136.5	13.48	30.04	0.97281
A3-1	Pegmatite	Muscovite	758	2.96	2100	19.30836
Shahmon pluton						
A57	Monzogranite	WR	81.66	408.3	0.5788	0.70905
A99	Monzogranite	WR	111.5	381.7	0.8454	0.71179
A97	Pegmatite	WR	229.8	67.17	9.985	0.79567
A98	Monzogranite	Muscovite	1362.2	5.885	1670.3	15.86586

Eu/Eu* and Sr suggest that plagioclase settling played the dominant role in this process.

Mass-balance calculations, based on least-square modeling of fractional crystallization were performed. Average chemical composition of the least fractionated rocks (monzogranite from the Mt Rehavam area) was taken as the parental magma. The major-element modeling was tested by Rb, Ba, Sr and Eu, which reside dominantly in major mineral phases in the granitic system. The best result was obtained for a version

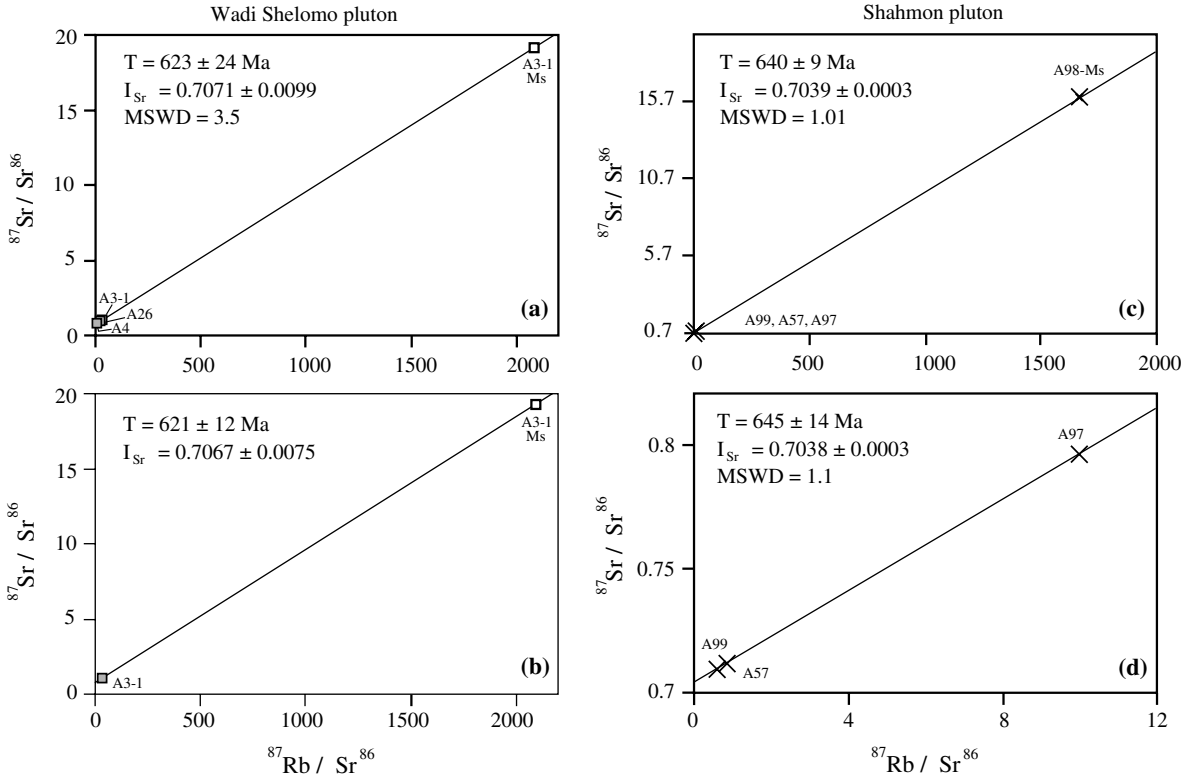

Fig. 9. Rb-Sr isochron diagrams of monzogranites from the Wadi Shelomo and Shahmon plutons.

Table 9
Values of $\delta^{18}O$ of minerals from Elat Granite and Shahmon Gneissic Granite

Sample no., rock, area	Quartz	Zircon	Garnet
Elat Granite			
Wadi Shelomo pluton			
YE-11	10.38		6.55 ± 0.02
YE-31 (aplite)	10.23		6.61
YE-32 (pegmatite)	10.09		6.52
YE-33	10.31	6.97	
Rehavam pluton			
YE-30 (Wadi Roded)	11.17		
YE-34 (Mt Rehavam)	10.71		
Shahmon Gneissic Granite			
YE-28	11.22		
YE-29	11.32		

YE-11 garnet was duplicated and average listed above.

assuming fractionation of plagioclase to the extent of about 16 wt% (Table 11).

9.4. Age of gneissic granite from the Shahmon pluton

The Rb–Sr date obtained for SGG leaves room for two possibilities of its interpretation. SGG and EG have the same age within arror brackets: 640 ± 9 Ma and 623 ± 24 Ma, respectively. Considering these data, as well as similarity of SGG and EG in modal composition, mineral and whole-rock chemistry (Figs. 2, 3, 5–7; Tables 1, 2, 5–7), we can assume that these two granites formed simultaneously from magmas of similar composition. However, SGG was later subjected to tectonic effect within a shear zone, and as a result, gneissic texture was developed in this rock. Unfortunately, small dimensions of the cropped out area do not allow us to find compelling proof to this hypothesis. The only evidence of possible influence of a shear zone is presence within the Shahmon pluton of both weakly and strongly gneissic granites that are characterized by indistinguishable composition, clear contact, but no crosscutting relations.

The other hypothesis is based on the assumption that gneissic texture of granite and subsolidus alteration of magmatic muscovite in SGG (Fig. 4) points to metamorphic event that occurred 640 ± 9 Ma. Such an assumption is supported by data on widespread deformation and metamorphism reported in Sinai and southern Israel at the same period, 650–640 Ma (Eyal et al., 1991; Garfunkel, 2000). Metamorphism at this stage may have reset some ages, e.g. a 645 Ma Rb–Sr date of the 780 Ma old Fjord Gneiss (Bielski, 1982) and the Ar/Ar date of 646 Ma of biotite in the 745 Ma old Elat Granitic Gneiss (Heimann et al., 1995). Thus it is quite possible that emplacement of SGG occurred during or shortly before the metamorphic event, at the very beginning of the post-collision batholithic stage or even at the

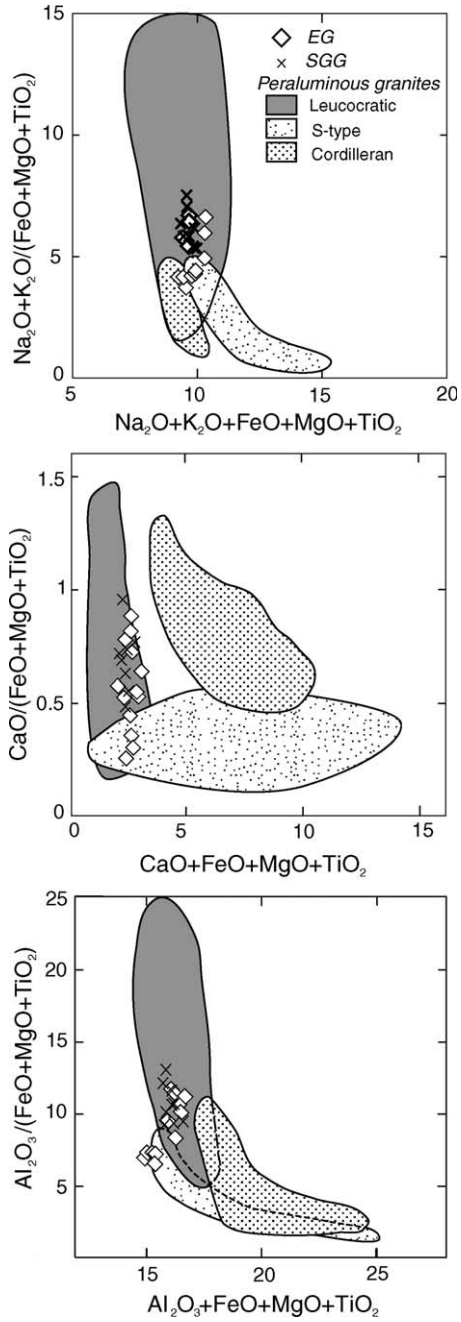

Fig. 10. Compositions of the EG and SGG compared to the fields of three peraluminous granite types (field contours are drawn according to the data of Patiño Douce, 1999).

end of the island arc stage, as suggested for the peraluminous garnet-bearing leucogranite from the Wadi El-Hudi area in the south Eastern Desert, Egypt (Moghazi et al., 2001).

9.5. Elat granite and Younger granites II in Egypt

Calc-alkaline Younger Granites II are abundant among the Neoproterozoic granitic rocks in the Sinai Peninsula and the Eastern Desert, Egypt (e.g., El-Mettwaly et al., 1992; El-Sheshtawi et al., 1993; Furnes et al., 1996; Moghazi, 1999, 2002; Abdel-Rahman and El-Kibbi, 2001). Like the EG, they formed after the emplacement of the diorite-tonalite-granodiorite suite (Older Granites I), but before that of the alkaline

Table 10
Temperature estimate for the Rehavam pluton monzogranites and the enclosing biotite-garnet schist from contact zones (°C)

Sample no., rock, area	Pressure (kbar)		Minerals	Source
	2	4		
Monzogranite				
Mt Rehavam area				
A38	761	793	Bi + Mu	1
A102	770	801	Bi + Mu	1
Wadi Roded area				
A48	711	742	Bi + Mu	1
A41	680	710	Bi + Mu	1
The enclosing schist				
Wadi Roded area				
A107-1	640	646	Bi + Grt	2
	640	642	Bi + Grt	3
Wadi Shelomo area				
A34	627	634	Bi + Grt	2
	616	618	Bi + Grt	3

Source: 1—Hoisch (1989), precision ± 40 °C, 2—Kleemann and Reinhardt (1994), 3—Bhattacharya et al. (1992), reformulated improvements over existing Bi-Grt geothermometers.

Table 11
Results of least-square modeling of fractional crystallization of the Elat type granite magma, with the trace element testing

wt%	Parent Monzogranite	Daughter Monzogranite	
ppm	Mt Rehavam	Wadi Shelomo, average	
	Average	Observed	Calculated
SiO_2	73.84	76.05	75.59
TiO_2	0.14	0.15	0.17
Al_2O_3	14.97	13.49	13.61
FeO*	0.93	1.41	1.11
MnO	0.04	0.03	0.05
MgO	0.38	0.18	0.46
CaO	0.96	0.80	0.53
Na_2O	4.93	3.98	4.02
K_2O	3.75	3.86	4.39
P_2O_5	0.06	0.05	0.07
Rb	93	100	109
Ba	571	633	642
Sr	383	99	115
Eu	0.61	0.51	0.51
Fractionating mineral, wt%		Plagioclase (An_{15})	15.9
Residual melt, wt%			84.1
Sum residuals squared			0.755

Major elements are recalculated to total = 100% volatile free. Total Fe as FeO*. Partition coefficients for Rb and Sr after Nash and Crecraft (1985); K^D for Ba and Eu after Arth (1976).

granites (Younger Granites III) and are considered as late post-collision. Mostly these rocks formed during the time span of 600–570 Ma (Fullagar and Greenberg, 1978; Fullagar, 1980; Bielski, 1982; Stern and Hedge, 1985).

The compiled data on chemical composition of these granites indicate that they are calc-alkaline and mostly high-K and incorporate both metaluminous and peraluminous types (Fig. 11). Close spatial and temporal association of peraluminous and metaluminous granites as occurred in the Sinai Peninsula and the Eastern Desert is not unusual. It had been argued that intrusion of such two types of granites is possible during post-collisional stages, if extensive melting occurred in a <50 km thick crust (Sylvester, 1998). According to McGuire and Stern (1993), lower-crustal granulite in the Neoproterozoic Arabian-Nubian Shield formed at $P \leqslant 12$ kbar. This suggests that crust thickness was ~40 km. Compositions of peraluminous granites from Sinai and Eastern Desert overlap the EG field (Fig. 11). Similarity of EG and peraluminous varieties of the Younger Granite II suggests that the late to post-collision magmatic event affected an extensive region in the northern part of the Arabian-Nubian Shield (see Inset in Fig. 1).

9.6. Possible sources of the EG and SGG magmas

A predominance of crustal sources is generally assumed for peraluminous granites. Three models are suggested: (1) melting of metapelite and metagreywacke, including cases of basalt magma admixture (White and Chappell, 1988; Sylvester, 1998; Patiño Douce, 1999); (2) partial melting of tonalite and granodiorite at pressures $\geqslant 8$ kbar with clinopyroxene in restite (Patiño Douce, 1997, 1999); (3) evolution of relatively primitive low-Ca metaluminous granites by fractionation of amphibole (Bonin et al., 1998).

Unfortunately, the geological and geochemical evidence is inadequate to allow us to discuss origin of EG and SGG in the context of all three above mentioned models. It is commonly accepted that the most important evidence for the granitic magma source is provided by radiogenic isotopes, e.g., Rb–Sr and Sm–Nd studies. However, predominance of young juvenile crust in the Arabian-Nubian Shield at the time of generation of the SGG and EG magma does not allow one to distinguish between crustal- and mantle-derived sources on the basis of isotope data (Bentor, 1985; Stern and Kröner, 1993; Stein and Goldstein, 1996; Stern and Abdelsalam, 1998). For example, the $\varepsilon_{Nd}(T)$ values in metamorphic rocks, granites and rhyolites from different parts of the Arabian-Nubian Shield range from +7.6 through +3.5, among them +3.6 in the Wadi Shelomo pluton (Stein and Goldstein, 1996). These values are usually considered to be characteristic of more or less depleted mantle. Under these circumstances it is hardly possible to estimate the ratio of crustal and mantle-derived components in the silicic magmas. Rough estimate can be done on the

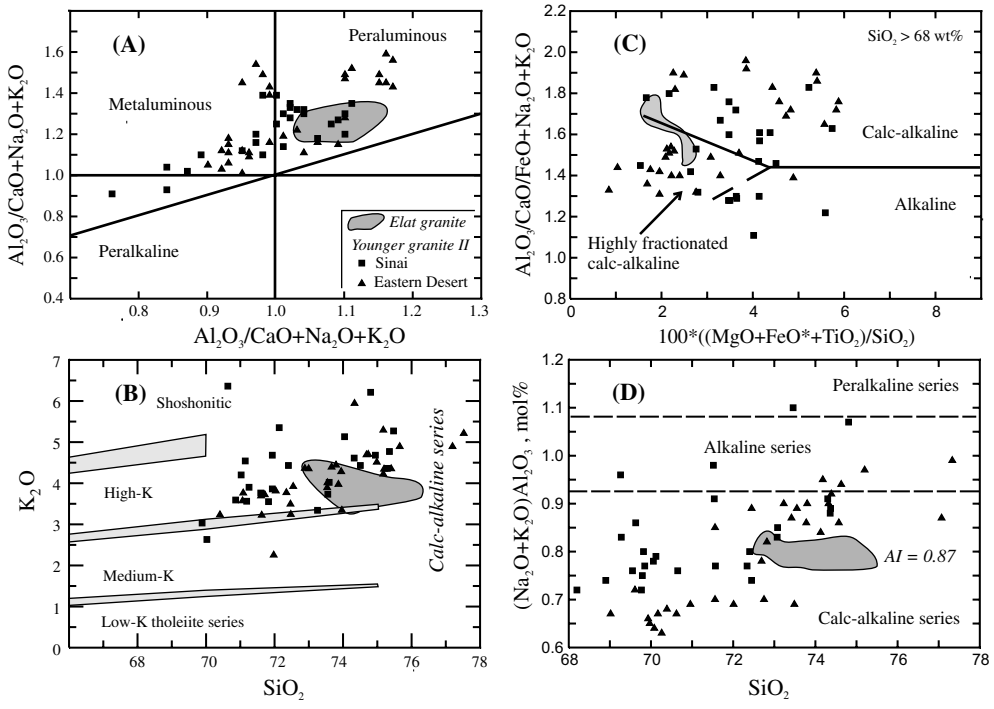

Fig. 11. Comparison of the EG (shaded area) with the Pan-African late to post-collision calc-alkaline granites from the Sinai Peninsula and the Eastern Desert, Egypt (see references in the text). A and B as in Fig. 5; C = major element discrimination of post-collision granites (from Sylvester, 1989); D = Agpaitic index (*AI*) vs SiO_2 (from Liégeois et al., 1998).

basis of new oxygen isotope ratios. It was shown in Section 8 that for EG the whole-rock $\delta^{18}O$ values calculated in accordance with data on whole-rock-zircon and whole-rock-quartz fractionation is ~9‰. This value is significantly higher than typical bulk mantle estimate, 5.5‰ (Mattey et al., 1994) and MORB $\delta^{18}O$ values of 5.7 ± 0.2‰ (Harmon and Hoefs, 1995; Eiler et al., 2000). On the other hand, the calculated whole-rock EG $\delta^{18}O$ value is near the lower limit of $\delta^{18}O$ value for modern and Proterozoic clastic deposits that range from 9 to 15‰ (Taylor and Sheppard, 1986). This gives ground to consider that proportion of crustal component in the EG was substantial, no less than 50%.

Some petrogenetic information can be obtained from the diagrams illustrating correlation of the granite compositions with compositions of melts produced by experimental dehydration melting of various types of crustal rocks (Patiño Douce, 1999). In Fig. 12, EG and SGG samples plot within the fields of felsic pelite and greywacke-derived magma. Abundance of metapelites with

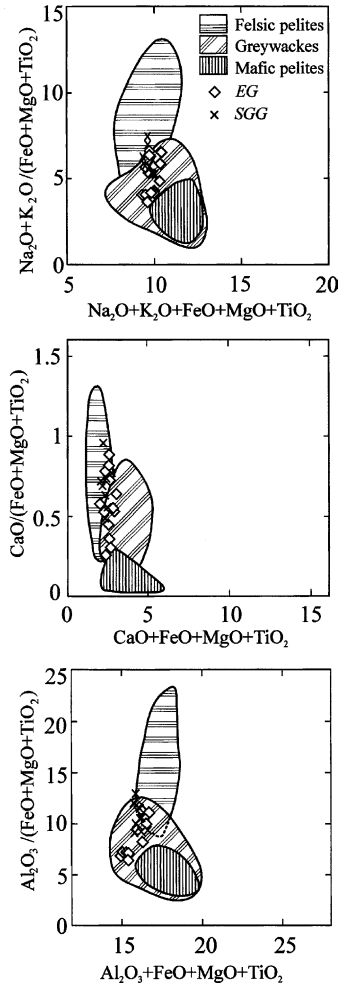

Fig. 12. Compositions of the EG and SGG compared to melts produced by experimental dehydration melting of metasedimentary rocks (fields of melt compositions after Patiño Douce, 1999).

sillimanite, andalusite, garnet, cordierite in southern Israel (Shimron, 1972; Matthews et al., 1989; Katz et al., 1998) and throughout the Sinai Peninsula (Bentor, 1985) supports this hypothesis. Also, it was established for some typical leucogranite plutons studied in detail, such as Manaslu pluton and network of leucogranite sills in Nepal (Le Fort, 1981 and references therein; Inger and Harris, 1993; Guilot and Le Fort, 1995), Harney Peak in South Dakota, USA (Nabelek et al., 1992), the Trois Seigneurs Massif, Pyrenees, France (Wickham, 1987), that silicic magma was produced by partial melting of crustal rocks. Hence, we can assume Al-rich crustal rocks as the source of the peraluminous leucocratic Elat and Shahmon granite magmas. Thus, model 1 seems realistic. It is worth noting that models similar to above models 2 and 3 were proposed to account for the origin of granite magmas that formed some types of the Young Granites II in the Eastern Desert, Egypt: the Daneiba peraluminous leucogranite, subsolvus syenogranite at Shalatin-Halab, and granodiorite from tonalite-granodiorite suite in the Homrit Waggat and El-Yatima areas (El-Sayed and Nisr, 1999; Moghazi et al., 1999; El-Nisr et al., 2001).

10. Conclusions

1. Two groups of peraluminous, high-K calc-alkaline granites have been distinguished in southern Israel: coarse-grained massive Elat monzogranite, and gneissic fine- to medium-grained Shahmon monzogranite.
2. Rb-Sr isotope dating suggests that the EG emplacement occurred at 623 ± 24 Ma, at the end of the post-collision batholithic stage. Unfortunately, due to the high error, time of emplacement is poorly constrained. Data on the age of SGG are still ambiguous.
3. Peraluminous granites, similar to the EG, are widespread among the Younger Granite II plutons in the Sinai Peninsula and the Eastern Desert, Egypt.
4. The most appropriate model of the EG and SGG magma generation is assumed to be partial melting of metapelite and greywacke crustal rocks.
5. In the EG type, a noticeable distinction in chemistry and mineral composition between rocks making up the Rehavam and the more differentiated Wadi Shelomo plutons was caused by fractional crystallization of granite magma at temperature of about 760–800 °C.

Acknowledgement

This research was supported by Israel Ministry of Energy and Infracrtucture, grant #81976201 and by Israel Science Foundation, grant #82130101. We thank

J. Valley and M. Spicuzza for help with oxygen isotope analysis. We are deeply grateful to reviewers Ahmed A. El-Metwally, J.P. Liégeois and A.B. Kampunzu for valuable recommendations and discussion that enabled to improve the manuscript. We also indebted R. Shagam for fruitful discussions and improvement of our English.

References

Abdel-Rahman, A.M., El-Kibbi, M.M., 2001. Anorogenic magmatism: chemical evolution of the Mount El-Sibai A-type complex (Egypt), and implications for the origin of within-plate felsic magmas. Geological Magazine 138, 67–85.

Ahmed, A.M., El Sheshtawi, Y.A., El Tokhi, M.M., 1993. Origin and geochemistry of Egyptian granitoid rocks in Nuweiba area, eastern Sinai. Journal of African Earth Sciences 17, 399–413.

Arth, J.G., 1976. Behaviour of trace elements during magmatic processes – a summary of theoretical models and their applications. U.S. Geological Survey Journal of Research 4, 41–47.

Bentor, Y.K., 1961. Petrographical outline of the Precambrian in Israel. Bulletin of the Research Council of Israel, Section G, 10G, 19–63.

Bentor, Y.K., 1985. The crust evolution of the Arabo-Nubian Massif with special reference to the Sinai Peninsula. Precambrian Research 2, 1–74.

Bentor, Y.K., Vroman, A., 1955. The geological map of Israel, Series A: the Negev, sheet 24: Elat. Geological Survey of Israel, Jerusalem.

Bhattacharya, A., Mohanty, L., Maji, A., Sen, S.K., Raith, M., 1992. Non-ideal mixing in phlogopite-annite binary: constraints from experimental data on Mg-Fe partitioning and reformulation of the biotite-garnet geothermometer. Contributions to Mineralogy and Petrology 111, 87–93.

Bielski, M., 1982. Stages in the evolution of the Arabo-Nubian Massif in Sinai. Ph.D. Thesis, the Hebrew University, Jerusalem, 155 p. (unpublished).

Bogoch, R., Bourne, J., Shirav, M., Harnois, L., 1997. Petrochemistry of a Late Precambrian garnetiferous granite, pegmatite and aplite, southern Israel. Mineralogical Magazine 61, 111–122.

Bonin, B., Azzouni-Sekkal, A., Bussy, F., Ferrag, S., 1998. Alkali-calcic and alkaline post-orogenic (PO) granite magmatism: petrologic constraints and geodynamic settings. Lithos 45, 45–70.

Brown, G.C., 1980. Calc-alkaline magma genesis: the Pan-African contribution to crust growth. In: Al-Shanti, A.M.S. (Ed.), Evolution and mineralization of the Arabian-Nubian Shield. Institute of Applied Geology, Jeddah, pp. 19–29, Bulletin 3.

Chappell, B.W., White, A.J.R., 1974. Two contrasting granite types. Pacific Geology 8, 173–174.

Cosca, M.A., Shimron, A., Caby, R., 1999. Late Precambrian metamorphism and cooling in the Arabian-Nubian Shield: Petrology and $^{40}Ar/^{39}Ar$ geochronology of metamorphic rocks of the Elat area (southern Israel). Precambrian Research 98, 107–127.

Druckman, Y., Weissbrod, T., Garfunkel, Z., 1993. Geological map of Israel, scale 1:100,000 (sheets 25 and 26 Elat). Geological Survey of Israel, Jerusalem.

Eiler, J.M., Baumgartner, L.P., Valley, J.W., 1992. Intercrystalline stable isotope diffusion: a fast grain boundary model. Contributions to Mineralogy and Petrology 112, 543–557.

Eiler, J.M., Schiano, P., Kitchen, N., Stolper, E.M., 2000. Oxygen isotope evidence for recycled crust in the sources of mid-ocean ridge basalts. Nature 403, 530–534.

El-Mettwaly, A.A., Zalata, A.A., Abu El-Enen, M.M., 1992. The evolution of the Pan-African granitoid rocks: geochemical evidences from SW Sinai massif, Egypt. Journal of African Earth Sciences 14, 111–119.

El-Nisr, S.A., El-Sayed, M.M., Saleh, G.M., 2001. Geochemistry and petrogenesis of Pan-African late- to post-orogenic younger granitoids at Shalatin-Halaib, south Eeastern Desert, Egypt. Journal of African Earth Sciences 33, 261–282.

El-Sayed, M.M., Nisr, S.A., 1999. Petrogenesis and evolution of the Dineibit El-Qulieb hyperaluminous leucogranite, Southeastern Desert, Egypt: petrological and geochemical constraints. Journal of African Earth Sciences 28, 703–720.

El-Sheshtawi, Y.A., Dardir, A.A., Khyamy, A.A., 1993. Petrography and geochemistry of granitic rocks, their origin and tectonic environment in the Wadi Risasa area, Southeastern Sinai, Egypt. Journal of African Earth Sciences 17, 497–511.

Eyal, M., Peltz, S., 1994. The structure of the Ramat Yotam Caldera, southern Israel: a deeply eroded Late Precambrian ash-flow caldera. Israel Journal of Earth Sciences 43, 81–90.

Eyal, Y., Eyal, M., Kröner, A., 1991. Geochronology of the Elat Terrain, metamorphic basement, and its implication for crustal evolution of the NE part of the Arabian-Nubian Shield. Israel Journal of Earth Sciences 40, 5–16.

Fleck, R.J., Greenwood, W.R., Hadley, D.G., Anderson, R.E., Schmidt, D.L., 1980. Rubidium-strontium geochronology and plate-tectonic evolution of the southern part of the Arabian Shield. In: United States Geological Survey Professional Paper 1131, 38 p.

Fullagar, P.D., 1980. Pan-African age granites of North Eastern Africa: new or reworked sialic materials? In: Salem, M.J., Busrewil, M.T. (Eds.), Geology of Libya, Second symposium on the Geology of Libya. Academic Press III, New York, pp. 1051–1058.

Fullagar, P.D., Greenberg, J.K., 1978. Egyptian Younger Granites: a single period of plutonism? Precambrian Research 6, Abstracts, p. A22.

Furnes, H., El-Sayed, M.M., Khalil, S.O., Hassanen, M.A., 1996. Pan-African magmatism in the Wadi El-Imra district, Central Eastern Desert, Egypt: geochemistry and tectonic environment. Journal of the Geological Society of London 153, 705–718.

Garfunkel, Z., 2000. History and paleogeography during the Pan-African orogen to stable platform transition: Reappraisal of the evidence from Elat area and northern Arabian-Nubian Shield. Israel Journal of Earth Sciences 48, 135–157.

Garfunkel, Z., Eyal, Y., Eyal, M., Weissbrod, T., Bakler, N., Shimron, A.E., Peltz, S., Gutkin, V., Bartov, Y., Drukman, Y., Rozenfeld, M., Sneh, A., 2000. Geological map of the Northern Gulf of Elat area, scale 1:100,000 (sheet 26 Elat). Geological Survey of Israel, Jerusalem.

Gass, I.G., 1982. Upper Proterozoic (Pan-African) calc-alkaline magmatism in North-eastern Africa and Arabia. In: Thorpe, R.S. (Ed.), Andesites and related rocks. Wiley, Chichester, pp. 595–609.

Genna, A., Nehlig, P., Le Goff, E., Gguerrot, Cc., Shanti, M., 2002. Proterozoic tectonism of the Arabian Shield. Precambrian Research 117, 21–40.

Guilot, S., Le Fort, P., 1995. Geochemical constraints on the bimodal origin of High Himalayan leucogranites. Lithos 35, 221–234.

Harmon, R.S., Hoefs, J., 1995. Oxygen isotope heterogeneity of the mantle deduced from global ^{18}O systematics of basalts from different geotectonic settings. Contributions to Mineralogy and Petrology 120, 95–114.

Heimann, A., Eyal, Y., Eyal, M., Foland, K.A., 1995. Thermal events and low temperature alteration in the Precambrian schistose dikes and their host rocks in the Elat area, southern Israel: $^{40}Ar/^{39}Ar$ geochronology. In: Baer, G., Heimann, A. (Eds.), Physics and chemistry of dykes. Balkema, Rotterdam, pp. 281–292.

Hoisch, T.D., 1989. A muscovite-biotite geothermometer. American Mineralogist 74, 565–572.

Holtz, F., Johannes, W., Tamic, N., Behrens, H., 2001. Maximum and minimum water contents of granitic melts generated in the crust: a reevaluation and implications. Lithos 56, 1–14.

Inger, S., Harris, N., 1993. Geochemical constraints on leucogranite magmatism in the Langtang Valley, Nepal Himalaya. Journal of Petrology 34, 345–368.

Johannes, W., Holtz, F., 1996. Petrogenesis and experimental petrology of granitic rocks. Minerals and Rocks 22. Springer-Verlag, pp. 115–275.

Katz, O., Avigad, D., Matthews, A., Heimann, A., 1998. Precambrian metamorphic evolution of the Arabian-Nubian Shield in the Roded area, southern Israel. Israel Journal of Earth Sciences 47, 93–110.

Kessel, R., 1995. The geochemistry of dykes and their host rocks from the latest stages of the Pan African orogeny, Amram and Elat massifs, southern Israel. MS thesis, the Hebrew University, Jerusalem, 121 p. (unpublished).

Kleemann, U., Reinhardt, J., 1994. Garnet-biotite thermometry revisited: the effect of Al^{vi} and Ti in biotite. European Journal of Mineralogy 6, 925–941.

Knowles, C.R., 1987. A basic program to recast garnet end members. Computers and Geosciences 13, 655–658.

Kröner, A., Eyal, M., Eyal, Y., 1990. Early Pan-African evolution of the basement around Elat, Israel, and the Sinai Peninsula revealed by single-zircon evaporation dating, and implications for crustal accretion rates. Geology 18, 545–548.

Le Fort, P., 1981. Manaslu leucogranite: a collision signature of the Himalaya, a model for its genesis and emplacement. Journal of Geophysical Research 86, 10545–10568.

Le Maitre, R.W. (Ed.), 1989. A Classification of Igneous Rocks and Glossary of Terms. Blackwell, Oxford, p. 193.

Liégeois, J.P., Navez, J., Black, R., Hertogen, J., 1998. Contrasting origin of post-collision high-K calc-alkaline and shoshonitic versus alkaline and peralkaline granitoids. The use of sliding normalization. Lithos 45, 1–28.

Ludwig, K.R., 2003. ISOPLOT, Version 3.00. A geochronological toolkit for Microsoft Excel. Berkeley Geochronology Center Special Publication 1, 70 pp.

Maniar, P.D., Piccoli, P.P.M., 1989. Tectonic discrimination of granitoids. Geological Society of America Bulletin 101, 635–643.

Mattey, D., Lowry, D., Macpherson, C., 1994. Oxygen isotope composition of mantle peridotite. Earth and Planetary Science Letters 128, 231–241.

Matthews, A., Reymer, P.S., Avigad, D., Cochin, J., Marco, S., 1989. Pressures and temperatures of Pan-African high-grade metamorphism in the Elat Association, NE Sinai. Israel Journal of Earth Sciences 38, 1–17.

McGuire, A.V., Stern, R.J., 1993. Granulite xenoliths from western Saudi Arabia: the lower crust of the late Precambrian Arabian-Nubian Shield. Contributions to Mineralogy and Petrology 114, 395–408.

Moghazi, A.M., 1999. Magma source and evolution of Late Neoproterozoic granitoids in the Gabel El-Urf area, Eastern Desert, Egypt: geochemical and Sr-Nd isotopic constraints. Geological Magazine 136, 285–300.

Moghazi, A.M., 2002. Petrology and geochemistry of Pan-African granitoids, Kab Amiri area, Egypt – implications of tectonomagmatic stages in the Nubian Shield evolution. Mineralogy and Petrology 75, 41–67.

Moghazi, A.M., Hassanen, M.A., Hashad, M.H., Mohamed, F.H., 2001. Garnet-bearing leucogranite in the El-Hudi area, southern Egypt: evidence of crustal anatexis during Pan-African low pressure regional metamorphism. Journal of African Earth Sciences 33, 245–259.

Moghazi, A.M., Mohamed, F.H., Kanisawa, S., 1999. Geochemical and petrological evidence of calc-alkaline and A-type magmatism in the Homrit Waggat and El-Yatima areas of eastern Egypt. Journal of African Earth Sciences 29, 535–549.

Mohamed, F.H., Hassanen, M.A., Matheis, G., Shalaby, M.H., 1994. Geochemistry of the Wadi Hswashia Granite Complex, northern Egyptian Shield. Journal of African Earth Sciences 19, 61–74.

Nabelek, P.I., Russ-Nabelek, C., Denison, J.R., 1992. The generation and crystallization conditions of the Proterozoic Harney Peak Leucogranite, Black Hills, South Dakota, USA: Petrogenetic and geochemical constraints. Contributions to Mineralogy and Petrology 110, 173–191.

Nash, W.P., Crecraft, H.R., 1985. Partition coefficients for trace elements in silicic magmas. Geochemica et Cosmochemica Acta 49, 2309–2322.

Patiño Douce, A.E., 1997. Generation of peraluminous A-type granites by low-pressure melting of calc-alkaline granitoids. Geology 25, 743–766.

Patiño Douce, A.E., 1999. What do experiments tell us about the relative contributions of crust and mantle to the origin of granitic magmas? In: Castro, A., Fernandez, C., Vigneresse, J.L. (Eds.), Understanding Granites: Integrating New and Classical Techniques. Geological Society Special Publications, 168, pp. 55–75.

Peck, W.H., King, E.M., Valley, J.W., 2000. Oxygen isotope perspective on Precambrian crustal growth and maturation. Geology 28, 363–366.

Rickwood, P.C., 1968. On recasting analyses of garnet into end member molecules. Contributions to Mineralogy and Petrology 18, 175–198.

Rickwood, P.C., 1989. Boundary lines within petrologic diagrams which use oxides of major and minor elements. Lithos 22, 247–263.

Rieder, M., Cavazzini, G., D'Yakonov, Yu.S., Frank-Kamenetsky, V.A., Gattard, G., Guggenheim, S., Kova, P.V., Müller, G., Neiva, A.M., Radaslovich, E.W., Robert, J.-L., Sassi, F.P., Takeda, H., Weiss, Z., Wones, D.R., 1999. Nomenclature of the micas. Mineralogical Magazine 63, 267–279.

Roobol, M.J., Ramsay, C.R., Jackson, N.J., Darbyshire, D.P.F., 1983. Late Proterozoic lavas of the Central Arabian Shield – evolution of an ancient volcanic arc system. Journal of the Geological Society, London 140, 185–202.

Shimron, A.E., 1972. The Precambrian structural and metamorphic history of the Elat area Ph.D. Thesis, the Hebrew University, Jerusalem, 244 p. (unpublished).

Spicuzza, M.J., Valley, J.W., Kohn, M.J., Girard, J.P., Fouillac, A.M., 1998. The rapid heating, defocused beam technique: A CO_2-laser based method for highly precise and accurate determination of $\delta^{18}O$ values of quartz. Chemical Geology 144, 195–203.

Stein, M., Goldstein, S.I., 1996. From plume head to continental lithosphere in the Arabian- Nubian Shield. Nature 382, 773–778.

Stern, R.J., Abdelsalam, M.G., 1998. Formation of juvenile continental crust in the Arabian-Nubian shield: evidence from granitic rocks of the Nakasib suture, NE Sudan. Geologische Rundschau 87, 150–160.

Stern, R.J., Hedge, C.E., 1985. Geochronologic and isotopic constraints on Late Precambrian crustal evolution in the Eastern Desert of Egypt. American Journal of Science 285, 97–127.

Stern, R.J., Kröner, A., 1993. Late Precambrian crustal evolution in NE Sudan: isotopic and geochronologic constraints. Journal of Geology 101, 555–574.

Stern, R.J., Sellers, G., Gottfried, D., 1988. Bimodal dike swarms in the North of the Eastern Desert of Egypt: Significance for the origin of the Precambrian ''A-type'' Granites in Northern Afro-Arabia. In: Greiling, R., Gaby, R. (Eds.), The Pan-African belt of NE Africa and adjacent areas: Tectonic evolution and economic aspects. Frieder, Vieweg, John, Braunschweig, Germany, pp. 147–179.

Sun, S., McDonough, W.F., 1989. Chemical and isotopic systematics of oceanic basalts: implications for mantle compositions and processes. In: Saunders, A.D., Norry, M.J. (Eds.), Magmatism in the Ocean Basins, Geological Society Special Publications, 42, pp. 313–345.

Sylvester, P.J., 1989. Post-collisional alkaline granites. Journal of Geology 97, 261–281.

Sylvester, P.J., 1998. Post-collisional strongly peraluminous granites. Lithos 45, 29–44.

Taylor, H.P., Sheppard, S.M.F., 1986. Igneous rocks: I. Processes of isotopic fractionation and isotope systematics. In: Valley, J.W., Taylor, H.P., O'Neil, J.R. (Eds.), Stable Isotopes in High-Temperature Geological Process, Mineralogical Society of America, Reviews in Mineralogy, 16, pp. 227–271.

Valley, J.W., 2001. Stable isotope thermometry at high temperatures. In: Valley, J.W., Cole, D. (Eds.), Stable Isotopes Geochemistry, Mineralogical Society of America, Reviews in Mineralogy, 43, pp. 365–414.

Valley, J.W., Chiarenzelli, J.R., McLelland, J.M., 1994. Oxygen isotope geochemistry of zircon. Earth and Planetary Science Letters 126, 187–206.

Valley, J.W., Kitchen, N., Kohn, M.J., Niendorf, C.R., Spicuzza, M.J., 1995. UWG-2, a garnet standard for oxygen isotope ratios: Strategies for high precision and accuracy with laser heating. Geochemica et Cosmochemica Acta 59, 5523–5531.

White, A.J.R., Chappell, B.W., 1988. Some supracrustal (S-type) granites from the Lachlan Fold Belt. Transactions of the Royal Society of Edinburgh, Earth Sciences 79, 169–181.

Wickham, S.M., 1987. Crustal anatexis and granite petrogenesis during low-pressure regional metamorphism: The Trois Seigneurs Massif, Pyrenees, France. Journal of Petrology 28, 127–169.

Wickham, S.M., Alberts, A.D., Zanvilevich, A.N., Litvinovsky, B.A., Bindeman, I.N., Schauble, E.A., 1996. A stable isotope study of anorogenic magmatism in East Central Asia. Journal of Petrology 37, 1063–1095.